JOURNAL OF GEOPHYSICAL RESEARCH, VOL. 96, NO. C9, PAGES 16,839–16,858, SEPTEMBER 15, 1991

Spatial and Temporal Variability of Global Surface Solar Irradiance

JAMES K. B. BISHOP

Lamont-Doherty Geological Observatory, Columbia University, Palisades, New York

WILLIAM B. ROSSOW

NASA Goddard Institute for Space Studies, New York, New York

A fast scheme for computing surface solar irradiance using data from the International Satellite Cloud Climatology Project (ISCCP) is described. Daily mean solar irradiances from the fast scheme reproduce the detailed global results from full radiative transfer model calculations to within 6 and 10 W m^{-2} over the ocean and land, respectively. In particular, the fast scheme reproduces the same dependence of surface irradiance on solar zenith angle which is critical for proper calculation of daily, seasonal, and latitudinal variability. Validation of both model results is limited because globally distributed data sets of high quality are lacking, particularly over the oceans. However, comparison of calculated monthly mean results using 5 months of ISCCP data (July 1983 to July 1984) with climatology from the 1970s at six temperate latitude ocean weather stations shows agreement within published estimates of interannual variability of monthly means at the individual stations. A further test against a 17-day time series at a continental site (43°N, 90°W, October–November 1986; 13–170 W m^{-2} range of irradiance), where ground and satellite data were spatially and temporally coincident, showed an accuracy of better than 9 W m^{-2} on a daily basis and less than 4% bias in the 17-day mean. Frequently used bulk formulae for solar irradiance were also evaluated in each of these tests. All suffered in comparison because they did not include a parameterization of the effects of the global variability in mean cloud optical thickness. Data from July (1983 and 1984) and January (1984 and 1985) were used to examine the spatial and temporal variability of surface irradiance and its potential impact on biospheric processes. Results show that the oceans and land experience fundamentally different light regimes, with continents receiving significantly greater irradiance. In summer, major interocean differences in zonally averaged irradiance are found in the northern hemisphere with the Atlantic greater than Pacific by up to 80 W m^{-2}; in the southern hemisphere, interocean differences are small. Regional interannual variability (July 1983 versus 1984) ranged between +100 and −100 W m^{-2}. The variability, perhaps due to the 1982–1983 El Niño event, occurred mostly in the Pacific but extended beyond the tropics over the entire north Pacific basin. The nutrient-rich northern and southern ocean waters are almost perpetually cloud covered; however, there is a correspondence between higher than average surface irradiance and productivity in nutrient-rich areas of the southwest Atlantic and Weddell Sea sector of the circumpolar current. This suggests that solar irradiance must be considered as an important factor governing the productivity of these waters.

1. INTRODUCTION

Incident shortwave solar radiation at the Earth's surface is of fundamental importance to the Earth's biosphere and climate. Shortwave radiation is the prime energy source for terrestrial and marine photosynthesis and is a major term in the global surface heat budget. Solar irradiance also is important to geochemical cycling because both biological and photochemical processes strongly perturb distributions of chemical species on land and in the ocean. Clouds modulate surface solar irradiance. Consequently, there is a need to understand globally the spatial and temporal variability of cloudiness and how this variability impacts the biosphere, geochemical cycling, and climate. Such information is particularly needed for the ocean and for biospheric processes in general.

The photosynthetic fixation of inorganic carbon to organic matter is the dominant source of energy for the biosphere. However, there are fundamental differences in the way variability of solar irradiance affects photosynthesis on land and in the ocean. Unlike on continents, where plants are large and attached to the surface, marine plants are microscopic and are distributed vertically within a euphotic zone which extends from the surface to depths as great as 150 m. The vertical distribution of plant biomass on a day-to-day basis and the supply of nutrients to this sunlit zone are determined by water column stratification, vertical convective motions, and large-scale advection [e.g., *Sverdrup*, 1953]. These physical attributes of the euphotic zone are intimately connected to the daily fluctuations in air-sea heat balance [e.g., *Marra et al.*, 1990; *Bishop et al.*, 1991], of which solar irradiance is a major component. Unlike continental systems, where plant growth time scales are seasonal, marine plant populations can double in 1 day [e.g., *Sheldon et al.*, 1972; *Goldman and McCarthy*, 1978]. Thus the much smaller mass and shorter growth time scales for marine plants compared with land plants suggest that the day-to-day variability of solar irradiance has the potential to influence more strongly the distributions and production of biomass in the ocean than on land. A final factor distinguishing oceans from land is that precipitation from clouds is a critical source of water for all biological processes on land.

On land, variations in photosynthetic activity has been estimated using the normalized difference vegetation index (NDVI) derived from advanced very high resolution radiometer (AVHRR) data [*Tucker and Sellers*, 1986]. In the ocean, near-surface concentrations of phytoplankton pigments have been mapped on basin and global scales using the coastal zone color scanner (CZCS) [*Esaias et al.*, 1986; *Feldman et al.*, 1989]. Local and basin-scale models of ocean primary production using CZCS data are under development [*Platt*, 1986; *Bidigare et al.*, 1987; *Wroblewski et al.*, 1988; *Sathyendranath and Platt*, 1988; *Sathyendranath et al.*, 1989; *Balch et al.*, 1989]; however, these efforts have relied either on locally measured solar irradiance values or on irradiance estimated on monthly time scales using climatological cloud cover and bulk formulae [e.g., *Budyko*, 1964; *Esbensen and Kushnir*, 1981; *Isemer and Hasse*, 1987; *Dobson and Smith*, 1988]. From a physiological point of view, the impact of the high-frequency variability of

Paper number 91JC01754.
0148-0227/91/91JC-01754$05.00

incident solar irradiance on the global distribution and species composition of phytoplankton has yet to be investigated, although it is well known that different plankton species differ in their growth response to light [e.g., *Langdon*, 1988]. Clearly, a better knowledge of the global spatial and temporal variability of surface solar irradiance can significantly improve our understanding of and ability to model the oceanic and terrestrial biospheres.

The distribution of clouds and their brightness is now one of the better remotely sensed properties of the Earth and have been used to compute surface solar irradiance. *Raschke et al.* [1987] used METEOSAT and GMS geostationary satellite data to compute incident solar radiation at the surface and found better than 10% agreement between computed monthly averages and measured fluxes at several hundred land stations. No comparisons were made over the ocean. *Stuhlmann et al.* [1990] used International Satellite Cloud Climatology Project (ISCCP) B2 (30 km resolution, uncalibrated) data from METEOSAT and investigated monthly variability of surface solar irradiance for the region bounded by 60°N, 60°S, 60°E, and 60°W for the years 1985 and 1986 and compared results with a similar grid of land stations as used by *Raschke et al.* [1987]. The agreement in monthly means with station data was similar to that found by *Raschke et al.* [1987]. *Chertok* [1989] used Nimbus 7 data to compute monthly solar irradiance over the ocean on a 9° x 9° grid (1000-km resolution at the equator). Errors of monthly means were estimated to range between 10 and 20 W m^{-2}. No data are reported over land.

The work presented here was motivated primarily by the need for an adequate global representation of the day-to-day variations of surface solar irradiance (250–4000 nm) and photosynthetically active irradiance (400–700 nm) for biosphere modelling purposes. A primary step toward satisfying these needs is the development of a fast computational scheme, valid for both ocean and land, for estimating the daily surface solar irradiance. The scheme developed uses C1 and CX data from the International Satellite Cloud Climatology Project. Briefly, ISCCP combines data from multiple geostationary and polar orbiting meteorological satellites to provide a global view of the occurrence and optical properties of clouds beginning with July 1, 1983 [*Schiffer and Rossow*, 1983, 1985; *Rossow et al.*, 1985; and *Rossow and Schiffer*, 1991].

2. Methods

2.1. ISCCP C1 and CX Data

The major input data set is the International Satellite Cloud Climatology Project C1 data, which contains, at nominal 2.5° x 2.5° resolution and every 3 hours for the globe, information about clouds, the atmosphere, and surface [*Rossow et al.*, 1988; *Rossow and Schiffer*, 1991]. Specific parameters used in the various models below are (1) solar zenith angle, (2) atmospheric ozone column abundance, temperature-humidity profile, tropopause temperature and pressure, and surface pressure (daily for each 2.5° region on the globe; from TIROS Operational Vertical Sounder (TOVS) data), (3) surface temperature and visible (at 0.6 μm) reflectance (every 3 hours for each 2.5° region), and (4) cloud parameters for a single layer: cover fraction, optical thickness (at 0.6 μm) and cloud top temperature and pressure (every 3 hours for each 2.5° region). Additional data sets employed are (1) ozone abundance profile climatology as function of month and latitude, (2) aerosol climatology for stratosphere and troposphere (including land-ocean difference), (3) land vegetation types and the ratio of their near-IR and visible albedos, (4) land-water fraction, and (5) snow and sea ice cover (every 5 days for each 1° region). The ISCCP CX data set is the high-resolution (4–8 km, subsampled at 30 km) data set used to generate C1 data. Although the ISCCP data are available eight times per day for most of the globe, regions not covered by geostationary satellite are observed less frequently by polar orbiters, leading to occasional gaps in the data. A limitation of the data is the fact that visible radiative retrievals are performed only when the solar zenith angle is less than 78.5°.

2.2. Full Radiation Transfer Model

The full radiative transfer model (referred to hereafter as FRT) was developed for use in the Goddard Institute for Space Studies (GISS) climate general circulation model (GCM) [*Hansen et al.*, 1983]. In the application here, ISCCP C1 parameters replace inputs from the other GCM physics subroutines [*Rossow and Lacis*, 1991; *Rossow et al.*, 1990]. The FRT model calculates the spectral variations of solar (and thermal) scattering and absorption in the atmosphere and at the surface. Model outputs are upward and downward total solar and thermal fluxes at the top of the atmosphere; at the tropopause; at the top and bottom of every atmospheric layer, including the cloud layer; at the top of the near-surface air layer; and at the surface for clear, totally cloudy, and fractionally cloudy, conditions. In addition, spectral solar fluxes corresponding to visible and near-IR bands and fluxes in the thermal "window" at 10–12 μm are reported, along with profiles of net flux and heating/cooling rates. Only calculations of downward solar fluxes are considered here with the total solar irradiance at the top of the atmosphere taken to be 1367 W m^{-2} [*Willson*, 1978].

For gaseous absorption, the correlated-k method [*Lacis and Oinas*, 1991] (see also *Lacis and Hansen* [1974]) is used to integrate over overlapping absorption bands. This method allows for accurate and efficient treatment of absorption in a vertically inhomogeneous atmosphere and for inclusion of variable scattering effects in the calculations. Needed parameters are obtained from an off-line calculation with a line-by-line model, using absorption coefficients tabulated by *McClatchey et al.* [1973] and *Rothman* [1981]. All radiatively significant atmospheric constituents are included: for solar radiation, these are H_2O, CO_2, O_2, O_3, and NO_2. Amounts of CO_2, O_2, and NO_2 were set by default to 1958 values but can be altered to represent any other year; H_2O and O_3 amounts are taken from ISCCP C1 data.

The full effects and vertical variations of atmospheric, aerosol, and cloud multiple scattering are included. Multiple atmospheric layers with arbitrary optical properties are combined using a "single Gauss point" version of the doubling equations, which, despite its name, handles angle integrations using two reference angles, allowing for separate treatment of the direct and diffuse radiation [*Hansen et al.*, 1983]. Needed scattering parameters are determined from off-line Mie computations [*Hansen and Travis*, 1974]. This approach accurately accounts for anisotropic reflection from the surface and clouds. Ocean directional albedo is based on a slightly modified version of the empirical model developed by *Minnis and Harrison* [1984]. Land directional albedos are approximated by the observed variation in the ISCCP C1 values of surface visible relectances with solar zenith angle. The spectral dependence of land surface albedos is specified in two parts covering the visible and near-IR portions of the spectrum, depending on vegetation type and snow/ice cover. Stratospheric and two kinds of tropospheric aerosols (one characteristic of ocean air and one characteristic of continental air) are included separately from clouds, based on the climatology of *Toon and Pollack* [1976].

Clouds can be described by two predetermined "microphysics" models, one representing liquid water clouds (effective particle size, 10 μm) and one representing ice clouds (effective particle size, 25 μm). These calculations use only the water cloud model to be

consistent with the radiative model used for the ISCCP retrievals. The cloud optical thickness values reported in the ISCCP data are measured at 0.6–μm wavelength. The radiative flux model includes the spectral variation of cloud scattering and absorption by referencing the optical parameters to those at 0.6 μm using the microphysical models. Thus specification of the cloud optical thickness at this single wavelength sets values of optical thickness (for scattering and absorption) at all wavelengths for the flux calculations.

The atmosphere is divided into as many as twelve vertical layers, up to eight in the troposphere and four in the stratosphere. The number of layers in the troposphere varies relative to seven standard layers (each a little more than 100 mbar thick) with the location of the tropopause, surface, and clouds. All clouds are represented by a single 100-mbar-thick layer with variable cover fraction and optical thickness which is inserted according to the cloud top temperature. Cloud base is constrained to be at least 20 mbar from the surface unless this causes the cloud to be less than 20 mbar thick, in which case the cloud extends to the surface.

The present calculations were performed for July 1 and July 31, 1983, on the standard 2.5° x 2.5° grid used to display ISCCP C1 data (these data are actually stored on an equivalent equal-area grid). To obtain daily average solar fluxes, the linear average of the eight times per day calculations is scaled by the ratio of the theoretical, diurnal average of the cosine of the solar zenith angle to its actual average value for the data used. The theoretical value is based on an astronomical calculation of solar zenith angles every half hour for each day at each latitude. This ratio weights the resulting averages according to the portion of the day actually observed; however, weighting the result by the ratio of the illuminating fluxes does not weight the variations of atmospheric transmissivity and reflectivity with solar zenith angle. The effect of the weighting is not important for locations with all 3-hourly samples available, however.

2.3. *Computationally Fast Scheme*

The full radiative transfer scheme above is computationally intensive (40 min CPU per day of data), and it was thought that significant speed improvement could be realized because the "solar" portion of the spectrum is simpler in its radiation transfer characteristics than the thermal infrared and we are interested only in surface solar irradiance. The philosophy behind the development was to begin with simple parameterizations of clear sky and cloudy sky irradiances and to introduce complexity only to the level required by the physics. The resulting simplified scheme is 100 times faster than the FRT model on the same computer.

The fast algorithm for surface solar irradiance (referred to hereafter as FAST) utilizes the following ISCCP data: solar zenith angle (μ_o), atmospheric water vapor profile (H_2O) and ozone column abundance (O_3), cloud fraction (CF), cloud optical thickness (τ), visible surface reflectance (R_S), surface type (land, water, coast, ice), and surface pressure (P_S). The major algorithm components are depicted in Figure 1 and equations (1)–(7). We begin with the computation of the clear sky component of solar irradiance:

$$Q_{CLR} = (1\text{-}CF)\ f(S_o,d,\mu_o^*,O_3,H_2O,R_S,Vis,P_S)\ W\ m^{-2} \quad (1)$$

$$Q'_{CLR} = (1\text{-}\overline{CF})\ f(S_o,d,\mu_o^*,O_3,H_2O,\overline{R}_S,Vis,\overline{P}_S)\ W\ m^{-2} \quad (2)$$

Q_{CLR} is the solar irradiance at the surface under clear sky conditions derived using the formula, f, of *Frouin et al.* [1989]. Q'_{CLR} based on daily averaged properties, is evaluated whenever the 3 hourly data are absent. The solar flux to the top of the atmosphere (S_o) is 1367 W m^{-2}. Corrections for seasonal variation in Sun-Earth distance (d) are included. The solar zenith angle (μ_o) averaged over the 3-hour period containing the ISCCP observation is denoted μ_o^*. Surface reflectance, R_S, is held constant at 0.06 over the ocean and set to the ISCCP (geographically varying) value over ice and land. This was done because sun glint contributes to oceanic values reported in ISCCP data. Visibility (Vis) is assumed constant at 25 km (but could be varied) and is the parameterization of aerosol effects.

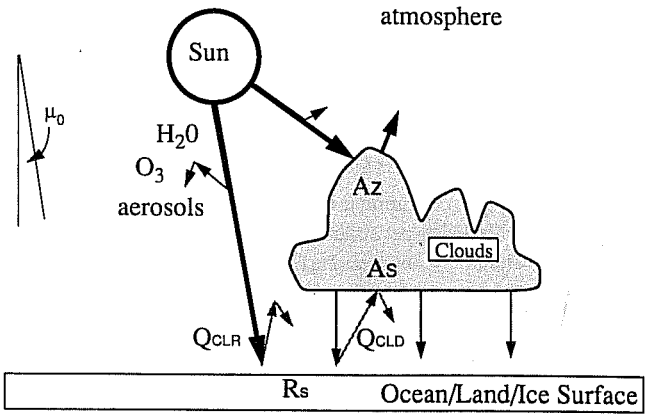

Fig. 1. Schematic representation of the components of the fast scheme for surface solar irradiance.

A comparison of zonal monthly averaged clear sky surface irradiance from *Berliand* [1960] and those computed using the *Frouin et al.* [1989] scheme using ISCCP data shows differences of only a few percent over land (Figure 2). This is consistent with the fact that Berliand's data were primarily land based. The advantage of the *Frouin et al.* [1989] formula is that it includes specific

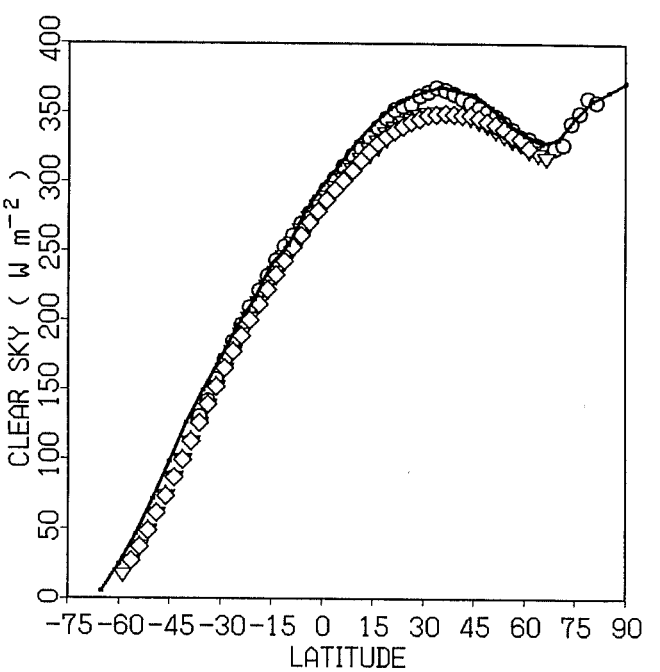

Fig. 2. July 1983 average clear sky surface irradiance over land (circles), Atlantic (inverted triangles), Indian (narrow diamonds), and Pacific (wide diamonds) oceans computed using *Frouin et al.* [1989] and ISCCP data compared with *Berliand*'s [1960] data. The results show little difference over land, consistent with Berliand's data being primarily land derived.

parameterizations of the effects of variable surface reflectance, water vapor, ozone, aerosols, and surface pressure. Next we treat the cloudy sky component of irradiance:

$$Q_{CLD} = CF\, Q_{DIR}\, (1 - A_Z)\, (1 + A_S R_S)\ W\ m^{-2} \quad (3)$$

$$Q'_{CLD} = \overline{CF}\, Q_{DIR}\, (1 - \overline{A}_Z)\, (1 + \overline{A}_S \overline{R}_S)\ W\ m^{-2} \quad (4)$$

The cloudy sky component of the calculation (Q_{CLD}; equation (3)) begins with the direct solar flux to the cloud top (Q_{DIR}) which is Q_{CLR} evaluated with zero surface reflectance and zero cloud fraction. A fraction of that flux is reflected back to space using a solar zenith angle dependent cloud albedo, $A_Z(\tau, \mu_o^*)$. The remaining transmitted fraction exiting the cloud base, not absorbed by the surface (determined by surface reflectance, R_S), is reflected upward and is reflected downwards again from the cloud base (determined by spherical cloud albedo, $A_S(\tau)$). As in the clear sky case, Q'_{CLD} (equation (4)) is computed using daily averaged properties whenever a 3-hour ISCCP observation is missing.

The spherical (A_S) and directional (A_Z) albedos are related to the ISCCP optical thickness values at 0.6 μm. Although these albedos vary somewhat with wavelength over the whole solar band because of varying absorption by water, we can neglect this variation for two reasons. First, significant changes in the albedo occur only at wavelengths larger than 1.5 μm where there is much less solar radiation and much more absorption by water vapor. Thus these wavelengths contribute little to the total radiation at the surface. Second, in the presence of clouds, radiation at these longer wavelengths is absorbed by the cloud rather than by the water vapor; however, the difference in cloudy and clear surface irradiance is still very small. As we show by comparison of the FAST and FRT results, this approximation produces no systematic differences in results. Although we present our calculations of total solar irradiance in this paper, our objective is to study the variability of PAR, for which this representation of the cloud albedos is nearly exact.

Rather than being computed in real time, A_S and A_Z are derived from cloud optical thickness using look-up tables provided by A. Lacis (Figure 3). These tables are obtained from full Mie calculations and provide the key physical link between the observed cloudy scene reflectance and the total cloud transmission which lies at the heart of all methods for calculating surface solar irradiances [e.g., *Tarpley*, 1979; *Gautier et al.*, 1980; *Darnell et al.*, 1988]. Use of look-up tables gives the FAST scheme a major improvement in speed while retaining most of the scattering physics.

The computation of total incident solar irradiance (Q_{TOT}) is the sum of clear (Q_{CLR}) and cloudy sky (Q_{CLD}) components (calculated every three hours) times a daily sampling correction factor (D).

$$D = \Sigma Q^*_{CLR} / \Sigma Q^{C1}_{CLR} \quad (5)$$

$$Q_{TOT} = D\ \Sigma(Q_{CLR} + Q_{CLD})\ W\ m^{-2};\ D < 1.3 \quad (6)$$

$$Q_{TOT} = \Sigma(Q_{CLR}+Q_{CLD}) + \Sigma(Q'_{CLR}+Q'_{CLD})\ W\ m^{-2};\ D > 1.3 \quad (7)$$

For D, the quantity Q^*_{CLR} is Q_{CLR} with CF = 0 and is evaluated every 3 hours if the sun is above the horizon and Q^{C1}_{CLR} is Q^*_{CLR} but is computed only when ISCCP C1 data are present (equation (5)). For most of the globe, the D ratio is close to unity (all eight ISCCP observations are present) because of extensive daily coverage by multiple geostationary and polar-orbiting satellites which contribute data to ISCCP; in this case, Q_{TOT} is evaluated using (6). When D is greater than 1.3 and the variation of incident solar irradiance with zenith angle is inadequately sampled, Q_{TOT} is derived by filling in the missing daytime values with clear and cloudy components computed using daily average cloud properties (equation (7)). This correction scheme differs from the solar zenith angle scheme used in FRT (section 2.2) in that corrections are based on the light field at the bottom of the atmosphere rather than at the top (FRT).

2.4. Bulk Formulae of Surface Irradiance

Three bulk formulae [*Budyko*, 1963; *Reed*, 1977; *Dobson and Smith*, 1988], widely used for global, ocean-scale, and local budgets of surface solar irradiance [e.g., *Budyko*, 1963; *Bunker*, 1976; *Esbensen and Kushnir*, 1981; *Reed*, 1985; *Isemer and Hasse*, 1987] are included in this comparison. All three formulae use only cloud fraction and empirically derived constants to compute the effects of clouds on surface solar irradiance. The Budyko and Reed formulae have been traditionally applied to monthly climatological data sets but, as formulated, can be equally applied to daily averaged data. The Dobson and Smith formula is formulated for hourly time scales. The *Budyko* [1963] formula was derived mainly using land

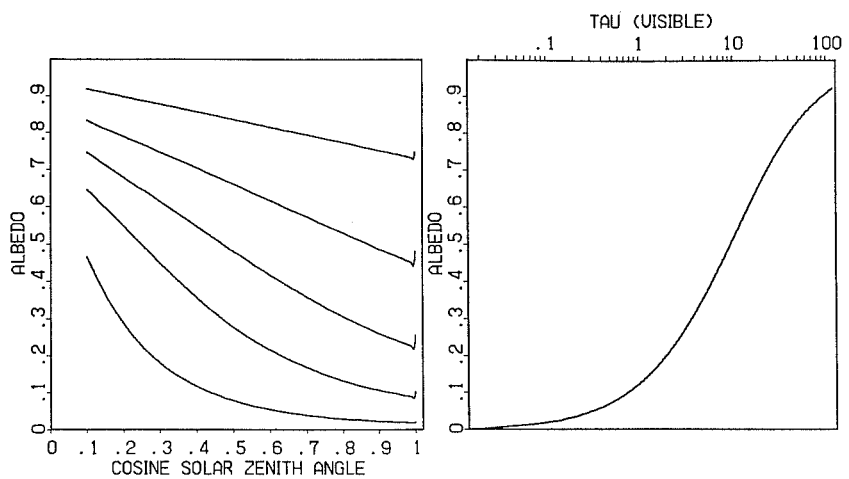

Fig. 3. (Left) Solar zenith angle dependent cloud albedo computed for clouds of optical thickness (0.51, 2.27, 5.94, 14.37, and 42.4, from bottom to top). These values correspond to the mean of each of five categories into which ISCCP further subdivides cloud data. The upward trend of albedo near cosine solar zenith angle of 1.0 is due to "glory" [see *Hansen and Travis*, 1974], which is an enhancement of backscatter due to an interference between grazing rays and noncentral rays which emerge after internal reflection within a cloud droplet. This effect is easily observed from aircraft. (Right) Spherical albedo as a function of cloud optical thickness. Cloud optical thickness values are for 600 nm.

surface observations but has been applied both over land and ocean; the *Reed* [1977] and the *Dobson and Smith* [1988] formulae were calibrated using data from several coastal weather stations and from ocean weather station P, respectively. They have been used only over the ocean. Our interest is in evaluating the performance of these formulae for computation of daily surface solar irradiance globally, since there is nothing in their formulation that prevents such an application.

The Budyko [1963] surface irradiance formula. The Budyko formula (referred to as BUDYKO) has been one of the most widely used methods depending on cloud fraction alone.

$$Q_{TOT}^{BUD} = S_o T \mu_o^D \{1 - aCF - bCF^2\} \text{ W m}^{-2} \quad (8)$$

Surface clear sky irradiance (Q_o), originally from *Berliand*'s [1960] monthly mean tabulations as a function of latitude, is replaced here by $S_o T \mu_o^D$ to facilitate daily calculations. The solar constant (S_o) is the same as in sections 2.2 and 2.3 above. Daily mean atmospheric transmission (T) equals 0.7402 (± 0.0091 s.d.) based on a fit of *Berliand*'s [1960] July monthly mean clear sky irradiance (Q_o) data from 45°S–55°N. The daily averaged solar zenith angle is μ_o^D. CF is cloud fraction averaged over daytime observations. Parameter a varies as a function of latitude and ranges between 0.35 and 0.41 from the equator to 55°N or S and decreases to 0.14 at the poles; parameter b is constant at 0.38. Corrections for Sun-Earth distance as a function of season are unnecessary, since Q_o values from Berliand include this effect.

The Reed [1977] ocean surface irradiance formula. Reed's formula (referred to below as REED) was recently used by *Reed* [1985] to estimate the heat budget of the tropical Pacific and by *Isemer and Hasse* [1987] in a revision of *Bunker*'s [1976] Atlantic heat budget calculations. Like the BUDYKO parameterization which it replaced, it uses daily averaged values for input. All terms are defined as in the BUDYKO formula with the exception of noon solar altitude, h (in degrees). Atmospheric transmission (T) is 0.7. *Isemer and Hasse* [1987] revised the multiplier for CF from Reed's 0.62 to 0.632. No correction for the variation of Sun-Earth distance is applied. Since the formula is linear in CF and h varies slowly over a month, there is no reason for this formula not to perform well on daily time scales.

$$Q_{TOT}^{REED} = S_o T \mu_o^D (1 - 0.632CF + 0.0019h) \text{ W m}^{-2} \quad (9)$$

The Dobson and Smith [1988] ocean surface irradiance formula. This formula (referred to hereafter as D&S), was calibrated using data from ocean weather station P (145°W, 50°N) from the 1960s and 1970s. It allowed for inclusion of the daily variation of solar zenith angle and cloud fraction and gave significantly better results than the BUDYKO formula over the ocean. Tests against other bulk formulae (including *Budyko* [1963] and *Reed* [1977]) showed that the D&S formula had better performance reproducing the day-to-day variability of solar irradiance both at station P and at five other temperate latitude ocean weather stations.

$$Q_{TOT}^{D\&S} = S_o \mu_o^* (A_i + B_i \mu_o^*) \text{ W m}^{-2} \quad (10)$$

A_i and B_i values are from Table 1 and i is oktas (0–8) of cloud cover (from CF rounded to nearest okta) for each 3-hour ISCCP observation. Cloud fraction is retrieved whenever the sun is above the horizon. No correction for Sun-Earth distance is applied for July (again because of calibration data being dominated by northern hemisphere summer). Correction for incomplete daily sampling is handled in an identical way as described in section 2.3 (equations (5)–(7)).

3. Model Evaluation

We evaluate the FAST scheme in three ways: (1) by global comparison with the FRT model results for July 1 and July 31, 1983; (2) by comparison to climatology at six ocean weather stations; and (3) by comparisons to a time series of surface measurements on land and to the results of four other satellite algorithms using simultaneously collected ISCCP CX data obtained during October–November 1986 [*Whitlock et al.*, 1990]. The first comparison tests the FAST parameterization against the FRT model, which explicitly includes all atmospheric and cloud radiative transfer physics. The key objective is to confirm that the FAST scheme properly handles variations with solar zenith angle. The second and third comparisons check the accuracy of both models. In all three comparisons, we also include results from the D&S, REED and BUDYKO bulk formulae applied to the same data. We acknowledge the fact that the D&S and REED, bulk formulae were calibrated using temperate latitude ocean and coastal data and therefore may be inappropriate over land. Similarly, Budyko's formula has a continental heritage. Our goal is to find a scheme which works well for daily surface solar irradiance both on land and over the ocean. Thus we compare bulk formula calculations to a full radiative transfer model and to our FAST scheme but break the comparisons down into categories including land and ocean.

3.1. Global Comparison: July 1 and July 31, 1983

We compare the global distribution of surface solar irradiance (Q_{TOT}), calculated using the FAST scheme, with the full radiative transfer (FRT) model results (and also with the BUDYKO, D&S, and REED bulk formulae) using ISCCP data from July 1, 1983, as input (Table 2, Figure 4). Regressions of the results from these calculations were performed after transforming the 2.5° x 2.5° girded data to an equal area (variable longitude by 2.5° latitude) basis to avoid areal biases. The comparison of FRT and FAST models shows globally (land, water, and ice surface) a slope of unity and standard deviation of 8 W m^{-2}. The majority of the visibly errant points (Figure 4*a*) occur over ice-covered land and ice-covered water. This suggests that improvements to the surface reflectance parameterization in the FAST scheme may be possible. Over the oceans, FAST versus FRT results (3461 points) again give a slope of 1 and a reduced standard error of 6 W m^{-2}. The slight positive intercept of 4 W m^{-2} can be explained by different parameterization of aerosols (held constant) and the different schemes for estimating daily integrals used by the two methods. FAST versus FRT comparisons using July 31 1983 data (not shown) as input yielded identical results.

Regressions of FAST versus FRT clear sky values for July 1 gave a standard deviation of 6 W m^{-2} for the globe, suggesting a 50%

TABLE 1. Coefficients for the *Dobson and Smith* [1988] Cloud Okta Model

	Okta								
	0	1	2	3	4	5	6	7	8
A	0.400	0.517	0.474	0.421	0.380	0.350	0.304	0.230	0.106
B	0.386	0.317	0.381	0.413	0.468	0.457	0.438	0.384	0.285

TABLE 2. Model Versus Model Intercomparison Statistics

Geographic Region	n	Slope	Intercept	Se(y)	R^2
			W m^{-2}		
		FAST Versus FRT			
Land	1676	0.9927 ± 0.0048	8.1± 1.3	10.1	0.9856
Coast	147	0.9976 ± 0.0178	5.6± 4.5	11.7	0.9834
Lakes+Seas+Arctic	373	1.0211 ± 0.0156	4.9± 4.0	13.3	0.9697
Atlantic Ocean	964	0.9962 ± 0.0026	5.8± 0.6	5.3	0.9976
Indian Ocean	697	1.0114 ± 0.0046	5.1± 0.8	6.3	0.9948
Pacific Ocean	1980	1.0062 ± 0.0025	3.1± 0.5	6.2	0.9954
All Global Areas	5837	1.0045 ± 0.0018	4.7± 0.4	8.3	0.9929
All Oceans	3641	1.0029 ± 0.0018	4.4± 0.3	6.1	0.9959
		FAST Versus D&S			
Land	1676	0.8941 ± 0.0166	32.0± 4.3	34.8	0.8242
Coast	147	0.9440 ± 0.0461	28.6±11.7	30.3	0.8879
Lakes+Seas+Arctic	373	0.8923 ± 0.0410	45.4±10.7	35.4	0.7761
Atlantic Ocean	964	1.0046 ± 0.0162	1.2± 3.5	32.7	0.9159
Indian Ocean	697	1.0197 ± 0.0179	-0.3± 3.2	24.6	0.9267
Pacific Ocean	1980	0.9957 ± 0.0123	7.6± 2.4	30.1	0.9002
All Global Areas	5837	0.9804 ± 0.0071	10.1± 1.6	32.4	0.8976
All Oceans	3641	1.0022 ± 0.0086	4.4± 1.7	30.0	0.9102
		FAST Versus REED			
Land	1676	0.8344 ± 0.0156	35.5± 4.1	32.7	0.8226
Coast	147	0.8774 ± 0.0500	30.6±12.7	32.9	0.8532
Lakes+Seas+Arctic	373	0.9023 ± 0.0378	31.1± 9.9	32.6	0.8065
Atlantic Ocean	964	0.8515 ± 0.0151	17.7± 3.3	30.7	0.8993
Indian Ocean	697	0.9006 ± 0.0178	7.7± 3.1	24.4	0.9089
Pacific Ocean	1980	0.8550 ± 0.0121	23.9± 2.4	29.6	0.8727
All Global Areas	5837	0.8799 ± 0.0069	20.0± 1.5	31.3	0.8831
All Oceans	3641	0.8618 ± 0.0084	19.2± 1.7	29.3	0.8868
		FAST Versus BUDYKO			
Land	1675	0.8902 ± 0.0218	-6.4± 5.7	45.7	0.7297
Coast	147	0.9200 ± 0.0749	-9.9±18.9	49.2	0.7403
Lakes+Seas+Arctic	373	0.8012 ± 0.0640	6.9±16.7	55.1	0.5349
Atlantic Ocean	964	0.7804 ± 0.0225	1.6± 4.8	45.5	0.7730
Indian Ocean	697	0.8235 ± 0.0270	1.8± 4.8	37.0	0.7844
Pacific Ocean	1980	0.8296 ± 0.0164	-5.9± 3.2	40.2	0.7786
All Global Areas	5836	0.8534 ± 0.0098	-5.2± 2.2	44.3	0.7802
All Oceans	3641	0.8088 ± 0.0118	-1.4± 2.3	41.2	0.7772

The ± symbol indicates 2σ estimate of uncertainty in slope and intercept values determined by least squares linear regression. Se(y), standard error of y.

contribution to the 8 W m^{-2} standard deviation in the comparison described above. This is mostly explained by the fact that the FRT method used ISCCP C1 values of μ_0 (instantaneous values at the time of the satellite observation) and a different scheme for deriving the daily average.

The above is a key test, since the data covers a variety of solar zenith angles during the day and as a function of latitude. Also ISCCP shows large differences in mean cloud properties between land and ocean and with location [*Rossow and Schiffer*, 1991]. From this, we conclude that the parameterization of cloud effects on surface irradiance in the FAST scheme is indistinguishable from that computed using the FRT model physics.

Fast versus bulk formulae. For convenience the FAST scheme is used as the basis of comparison with the three bulk formulae (Figure 4*b-d*). The breakdown of the data into "ocean" and "other (predominantly land)" categories in the figure allows a rapid visualization of how these formula perform in the contexts of "ocean" versus "land" calibrations. The FAST versus D&S regression (marginally cloudy pixels included) for the ocean gives a slope near unity (1.022) but a 5 times greater standard error (30 W m^{-2}) than FAST versus FRT. (Inclusion or exclusion of marginally cloudy pixels is based on performance of the various schemes in section 3.2 below.) Over land, the slope is 0.89, but a 32 W m^{-2} intercept offset is obtained. Similarly, the slope and standard error of the FAST versus BUDYKO land regression (marginal cloudy pixels excluded) are 0.89 and 46 W m^{-2}, respectively. It is notable that the BUDYKO regression is only slightly better over land than over the ocean and that the D&S regression is better over the ocean than on land. The REED formula shows overall poorer performance than D&S, and it is hard to see in the figure that its ocean performance is better than that over land. While the D&S regression results show positive intercepts only over land, the REED intercepts are positive everywhere.

3.2. Ocean Weather Stations

Monthly means and standard deviations of surface fluxes computed using the FAST scheme for the months July 1983, October 1983, January 1984, April 1984, and July 1984 were

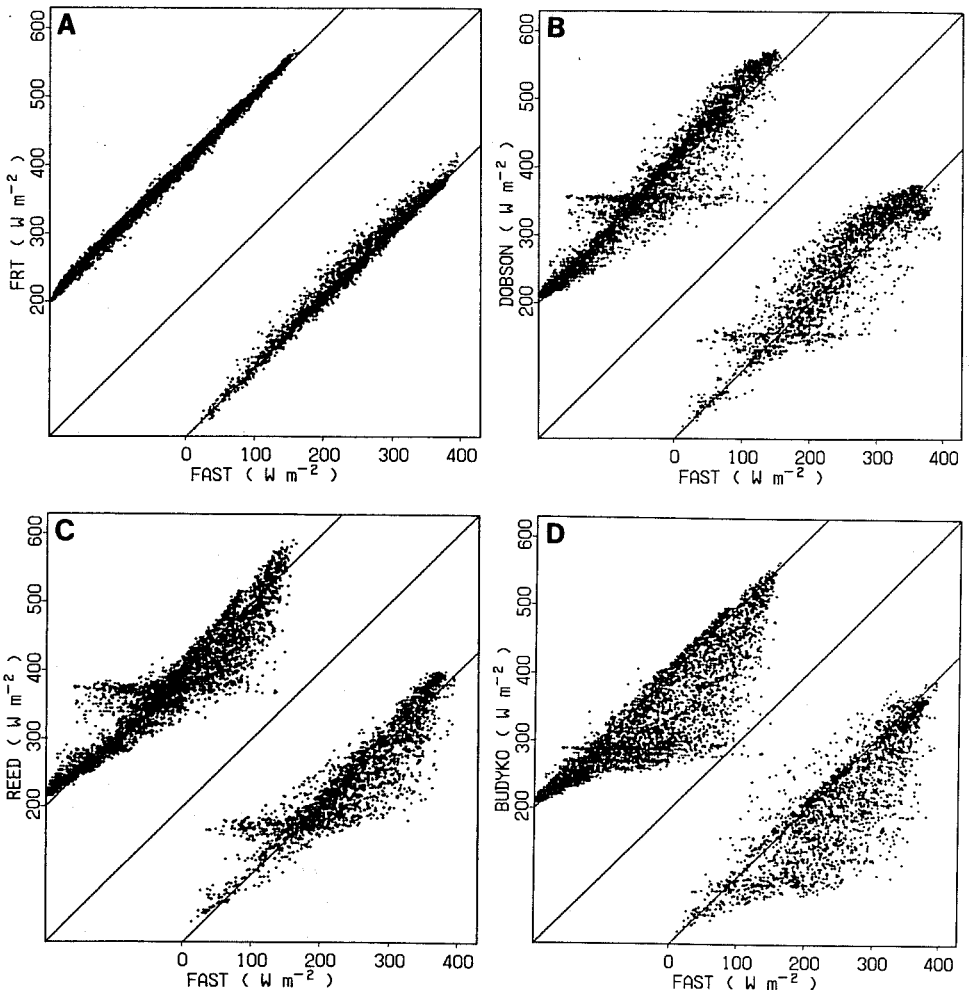

Fig. 4. (*a*) FAST scheme versus FRT model global solar irradiance comparison using ISCCP July 1 1983 data. (*b*) FAST scheme versus D&S formula comparison. (*c*) FAST scheme versus REED formula comparison. (*d*) FAST scheme versus BUDYKO formula comparison. Each graph is divided into "Atlantic+Pacific+Indian Oceans" (upper left) and "Land+Seas+Arctic" (lower right). 1:1 lines are drawn through the origin for each plot. A summary of linear regression statistics is found in Table 2. Clustering of data at a constant value on the *y* axes of Figures 4*b*, 4c, and 4*d* (particularly over the ocean) is due to a combination of (1) the fact that a large area of the ocean which is 100% overcast would receive nearly the same clear sky irradiance and (2) the lack of accommodation of variable cloud optical thickness in the bulk formulae. This is enhanced in the D&S case, since there are also quantization effects due to the use of oktas.

TABLE 3. Climatological (July 1970s) Versus Calculated Monthly Means (July 1983)

Station	Location	Obs.	BUDYKO(+ucpix)	REED (+ucpix)	D&S (+ucpix)	FAST (+ucpix)
OWS A	62.0°N,33.0°W	156	146±51 (139±47)	181±34 (178±32)	194±62 (188±63)	159±54 (157±53)
OWS B	56.0°N,51.0°W	174±28	138±77 (111±56)	194±54 (178±39)	204±71 (181±64)	190±91 (188±90)
OWS I	59.0°N,19.0°W	168	121±39 (111±29)	167±22 (162±15)	166±47 (156±37)	145±55 (143±54)
OWS J	52.5°N,20.0°W	178	111±57 (94±41)	178±37 (168±23)	178±58 (157±45)	179±58 (177±56)
OWS K	45.0°N,16.0°W	-	181±66 (147±56)	222±47 (201±40)	265±63 (228±68)	247±48 (244±48)
OWS P	50.0°N,145.0°W	173±22	127±60 (112±53)	186±36 (179±31)	191±53 (174±48)	167±53 (165±51)
SABLE I	44.0°N,60.0°W	236	187±86 (159±76)	231±60 (214±54)	253±76 (225±74)	231±80 (228±79)
model/obs mean			0.767 (0.658)	1.054 (1.002)	1.097 (1.003)	0.987 (0.974)
model/obs s.d.			0.104 (0.087)	0.074 (0.083)	0.099 (0.113)	0.075 (0.075)
average bias (W m^{-2})			-42 -62	10 0	18 1	-2 -5

All values in W m^{-2}. Obs. refers to climatological (1970s) means for A,I,J, and SI from *Dobson and Smith* [1988]; for B and P from *Smith and Dobson* [1984]. In the "Obs." column, ± indicates 2σ estimate for interannual variability of monthly means for OWS B and P. Elsewhere in the table, ± indicates standard deviation of July 1983 daily irradiance data; "+ucpix", values in the parentheses indicate the inclusion of the effects of marginally identified cloudy pixels and their optical thickness in the four schemes tested; model/obs mean is the average ratio of results from BUDYKO, REED, D&S, and FAST schemes to observed monthly means for the six stations compared; and s.d. is the standard deviation of the derived mean ratio.

compared with climatological data for ocean weather stations A, B, I, J, P, and Sable Island [*Smith and Dobson*, 1984; *Dobson and Smith*, 1988] representative of the 1960s and 1970s (Figure 5). Locations of stations (mostly in temperate latitudes) are found in Table 3. The comparison also includes one point for April 1982 for the region near 39°N, 72°W, from *Bishop et al.* [1991]. Linear regression results (±2 s.d. in parentheses) give a slope of 1.002 (0.082), intercept of 0.5 (11.6) W m^{-2}, and standard error of 17.5 W m^{-2}. The latter is consistent with the magnitude of interannual variability of monthly mean data reported by *Smith and Dobson* [1984] for stations B and P (Table 3; other stations not reported).

Sensitivity of the FAST, D&S, REED, and BUDYKO schemes to uncertainties in cloud fraction is also investigated at the same ocean weather stations using July 1983 ISCCP data and climatological mean data (Table 3). The four schemes were run using ISCCP data with and without the contributions of marginally cloudy pixels. The marginally cloudy pixels represent, for the most part, optically thin clouds which are just barely ("marginally") identified by the ISCCP cloud retrieval scheme. Such clouds may or may not be included in shipboard/land-based estimations of cloud cover which were the basis for the bulk formula parameterizations.

Consistent with the findings of *Dobson and Smith* [1988], the *Budyko* [1964] formula underestimates surface irradiance by 25 to 35%. The D&S formula is much more accurate than the BUDYKO formula, a yielding between 100% and 110% of the ground truth averages. The Reed formula yields between 100 and 105%. Like the BUDYKO formula, the D&S and REED results are sensitive to contributions of thin clouds to cloud fraction. Because the FAST scheme includes variable cloud optical thickness in addition to cloud fraction, the presence or absence of marginally cloudy pixels changes the results by only 2–3 W m^{-2}. This is because the effect of lowered cloud fraction is compensated by increased average cloud optical thickness.

We have already shown (Figure 5) that the FAST scheme reproduces the ocean weather station climatology within the limits of interannual variability. Although the FAST, D&S, and REED schemes (including marginally cloudy pixels) give nearly identical results for the monthly average of the six stations studied, they represent the variability of the daily irradiance at some stations very differently. This is examined below.

3.3. Wisconsin Experiment

The First ISCCP Regional Experiment/ Surface Radiation Budget (FIRE/SRB) experiment was carried out in a 100 km by 100 km region near 43°N, 89°W between October 14 and November 2, 1986 [*Whitlock et al.*, 1990]. This experiment permits algorithm validation over land in terms of the representation of daily variability of solar irradiance, since ground-based observations and ISCCP data are coincident in time and space (Figures 6 and 7). The daily averages of observations from the 12 land stations are compared with the results from computations utilizing 10 ISCCP CX pixels distributed over the same region. Since one or more daytime satellite observations were missing 10% of the time, there was also an opportunity to evaluate correction schemes for incomplete sampling. Regression of 17 days of ground observations and FAST estimates of daily radiation gives a slope of unity, 9 W m^{-2} rms error and -4 W m^{-2} bias (Table 4). The -4 W m^{-2} bias in the 17 day mean is not different from 0 at the 95% confidence level and is largely due to the single observation on day 306 where surface irradiance exceeded clear sky estimates by 10%. The FAST scheme also reproduces the variability of the fluxes over the 17-day period when Q_{TOT} ranged between 13 and 175 W m^{-2}. Nearly all aspects of FAST performance are slightly better than the satellite algorithms compared by *Whitlock et al.* [1990] (1–4, Table 4). This last statement should be qualified by the fact that the fast scheme was tested at a later date than the other algorithms; however, the FAST scheme also slightly betters the performance of the current version of the FRT model in this test.

The D&S, REED, and BUDYKO cloud okta formulae were significantly worse than all other methods compared. Consistent

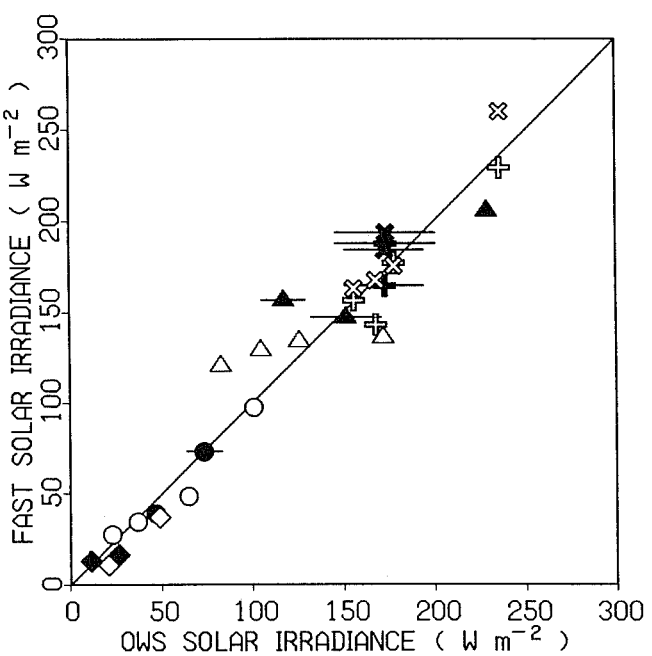

Fig. 5. Monthly mean solar irradiance from FAST scheme versus ocean weather station climatology from the 1970s. Symbols are as follows: pluses, July 1983; circles, October 1983; diamonds, January 1984; triangle, April 1984, and crosses, July 1984. Solid symbols and error bars (2 s.d. interannual variability) from *Smith and Dobson* [1984].

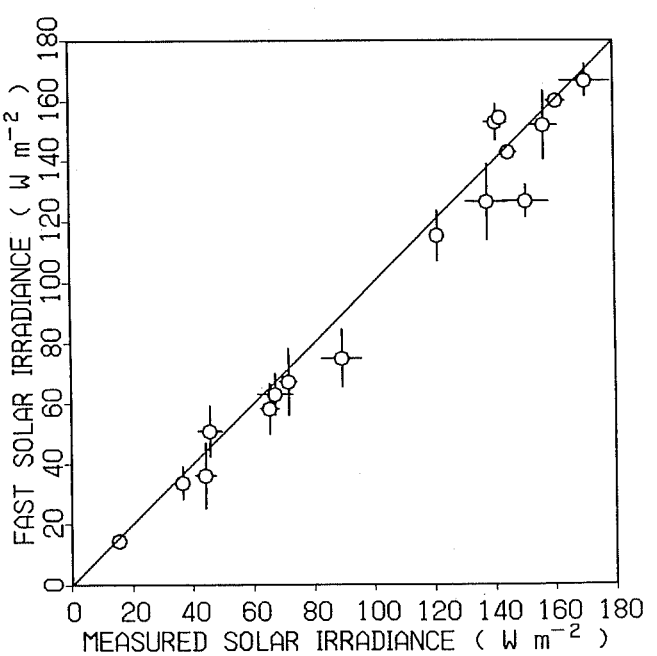

Fig. 6. FAST scheme versus data from FIRE/SRB Wisconsin experiment October 14 to November 2, 1986 [*Whitlock et al.*, 1990]. Error bars denote 2 s.d. for the means of 12 ground stations and results for the 10 ISCCP CX pixels distributed over the 100 by 100 km area of the experiment.

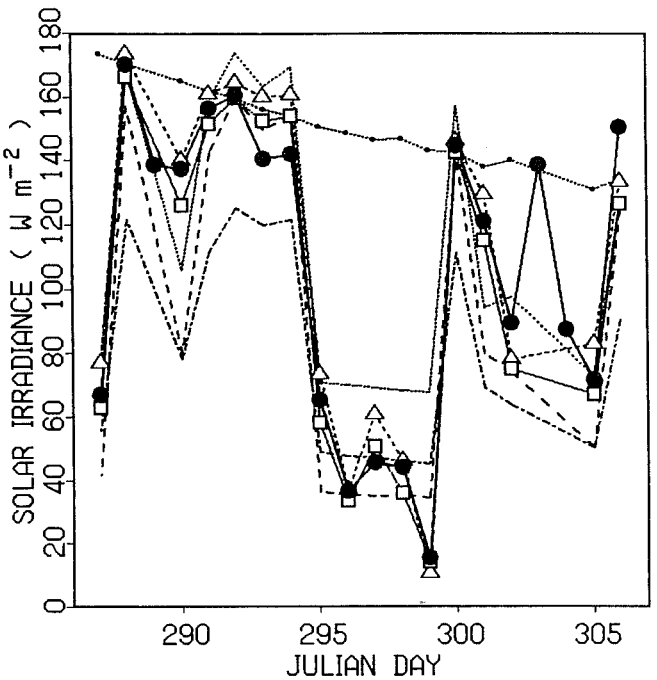

Fig. 7. Time series of surface solar irradiance during FIRE/SRB experiment. Symbols are solid circles, ground truth; open squares, FAST scheme; open triangles, FRT model; dot-dash line, D&S formula; dashed lines, BUDYKO formula; and dotted line, REED formula. Days 288, 303, and 304 lacked satellite observations. The small symbols denote clear sky irradiance calculated using the *Frouin et al.* [1989] formula, which for the most part agreed well with ground truth. The apparently anomalous ground truth point on Julian day 306 resulted from strong illumination from the sides of sparsely distributed but tall high-albedo clouds. Such effects are not parameterized in the FAST scheme, since they occur rarely.

with its land calibration, the BUDYKO formula reproduced the daily variability and 17-day mean much better than the D&S or REED formulae. The D&S formula underestimates clear sky irradiance at high solar zenith angles and overestimates irradiance during overcast conditions. REED overestimated both. The poorer performance of the D&S and REED formulae over land is consistent with their ocean heritage and the global comparison above (Table 2). This is not always true. The fact that *Bishop et al.* [1991] found that BUDYKO outperformed D&S in daily radiation budget calculations at a station in the NW Atlantic in April 1982 underscores the weakness of bulk formula parameterizations in their lack of accommodation of variable cloud optical thickness.

In summary, we conclude from the above tests that the FAST scheme (1) reproduces FRT model results globally to better than 9 W m^{-2} (6 W m^{-2} over the oceans) on a daily basis over an irradiance range of 0–400 W m^{-2} for all conditions (except over very bright surfaces), i.e., all sun angles, latitudes, and cloud types; (2) The FAST scheme versus ocean climatological data shows no serious biases (e.g., errors are < 10%); and (3) the FIRE/SRB test of the FAST scheme shows no serious bias over land and an accuracy of 9 W m^{-2} on a daily basis (13–170 W m^{-2} range). Of the bulk formulae, D&S appears to perform best in oceanic regions but could be improved for clear sky conditions. The BUDYKO formula is still best over land. *Dobson and Smith* [1988] noted that bulk formula parameterizations which incorporate cloud type in addition to cloud fraction did not perform any better than those depending on cloud fraction alone. These comparisons show that knowing cloud optical thickness in addition to cloud fraction immensely improves the estimation of surface solar irradiance. For irradiance calculations prior to July 1983 it may be possible to improve the bulk formulae by using ISCCP-based results to include the effects of regional variability of cloud optical thickness.

4. Results

4.1. Daily Statistics

We presented evidence in the introduction that oceanic primary production is more sensitive to day-to-day fluctuations of irradiance than terrestrial primary production. Given that the FAST scheme appears to represent accurately the daily fluctuations of surface irradiance (section 3), we proceed to use ISCCP data from July 1983 and January 1984 to ask two fundamental questions about the global variability of light: (1) Are there differences in the light regimes over land and the ocean? (2) Are there regions of the globe where the light field is persistent on a day-to-day basis and regions where it is not persistent? One approach to the first of these questions is simply to ask how many days of the month have surface solar irradiance exceeding 80% of that possible under clear skies. We choose 80%, since it corresponds to irradiance under approximately 50% cloud cover in the case of the FIRE/SRB experiment and a slightly greater fraction over the ocean. Below, we refer to days with irradiance less than 80% of clear sky values as "cloudy" and those with greater than 80% values as "clear."

Both the land and oceans have between 0 and 31 days per month

TABLE 4. Regression Statistics for FIRE/SRB Experiment Comparison

Model	n	Slope (±2σ), W m^{-2}	Intercept (±2σ), W m^{-2}	Se(y) (±1σ), W m^{-2}	R^2	17-day Mean (±1σ), W m^{-2}	Bias W m^{-2}	rms Error (±1σ), W m^{-2}
GT	17	-	-	-	-	103.7±51.1	-	-
1	17	1.0514 ± 0.0895	1.5±10.3	10.5	0.9656	110.6±54.7	6.9	10.5
2	17	1.0002 ± 0.0886	-4.7±10.2	10.4	0.9628	99.0±52.1	-4.7	10.0
3	17	0.9355 ± 0.0722	-0.0± 8.3	8.5	0.9715	97.0±48.5	-6.7	8.8
4	17	1.0107 ± 0.0924	4.4±10.6	10.8	0.9605	109.2±52.7	5.5	10.4
FRT	17	1.0048 ± 0.0851	3.8± 9.8	10.0	0.9659	108.0±52.3	4.3	9.7
FAST	17	0.9992 ± 0.0768	-3.7± 8.8	9.0	0.9718	99.7±51.8	-4.0	8.7
BU	17	0.9435 ± 0.1693	-7.6±19.5	19.8	0.8632	90.2±51.9	-13.5	19.4
D&S	17	0.5751 ± 0.1144	20.0±13.1	13.3	0.8371	79.7±32.1	-24.0	25.3
REED	17	0.7653 ± 0.1613	33.3±18.5	18.9	0.8207	112.6±43.2	9.0	21.9

Models are as follows: 1, Chou; 2, Gautier; 3, Pinker; 4, Rossow; GT, ground truth from *Whitlock et al.* [1990]; FRT, full radiative transfer model (section 2.2); FRT, updated version of 4 which included variation of Sun-Earth distance and a different parameterization of aerosols; FAST, fast scheme (section 2.3); BU, *Budyko* [1963]; D&S, *Dobson and Smith* [1988], REED, *Reed* [1977] formulae (section 2.4). Se(y), standard error of y; σ, standard deviation.

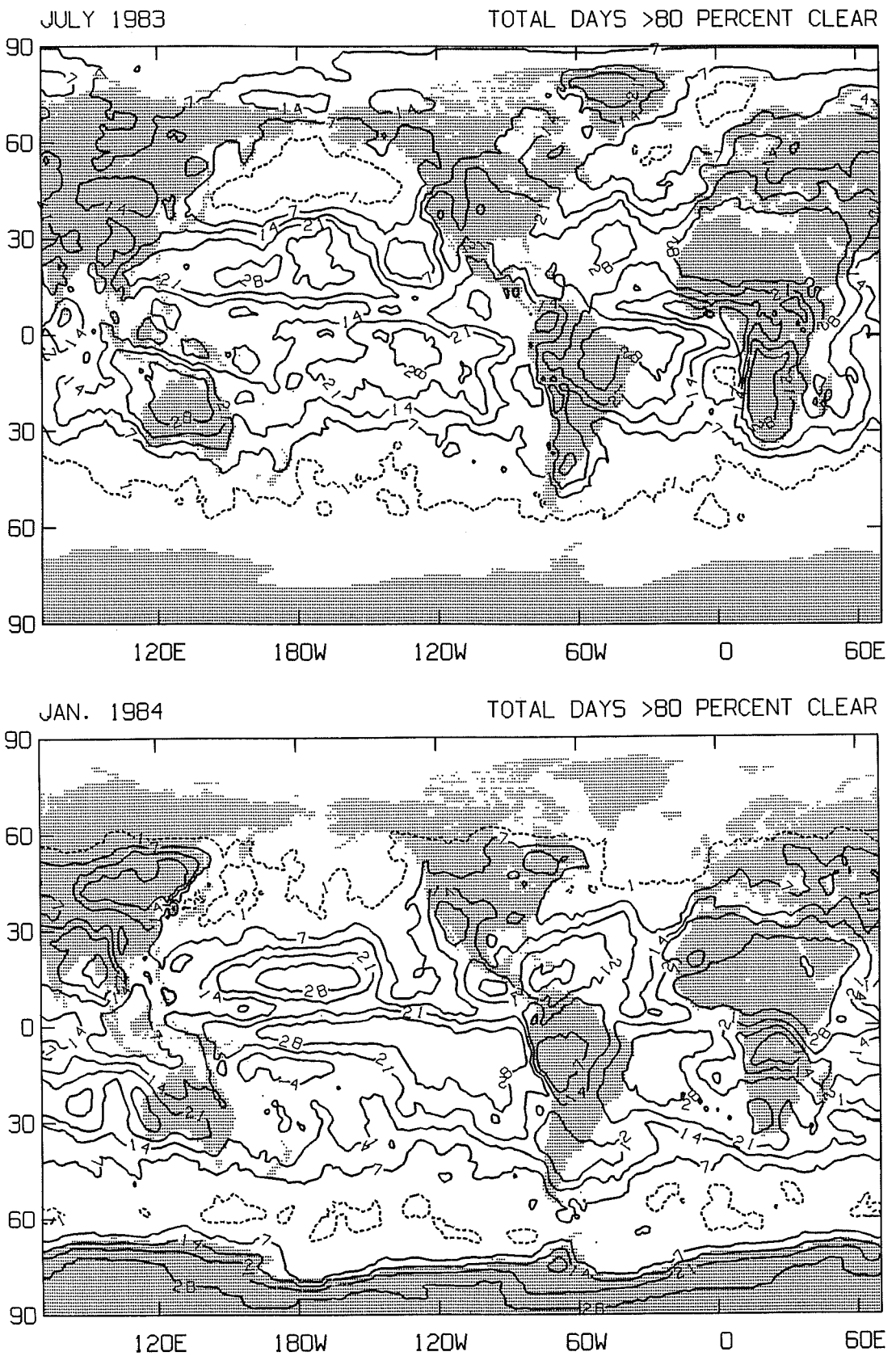

Fig. 8. (Top) Global map for July 1983 showing the number of days per month where surface irradiance exceeds 80% of that under clear sky. The 80% criterion corresponds roughly to 50% cloud fraction in the case of the FIRE/SRB experiment and slightly greater cover over the ocean. In July 1983, the North Pacific is significantly more cloudy than the North Atlantic. (Bottom) Similar data for January 1984.

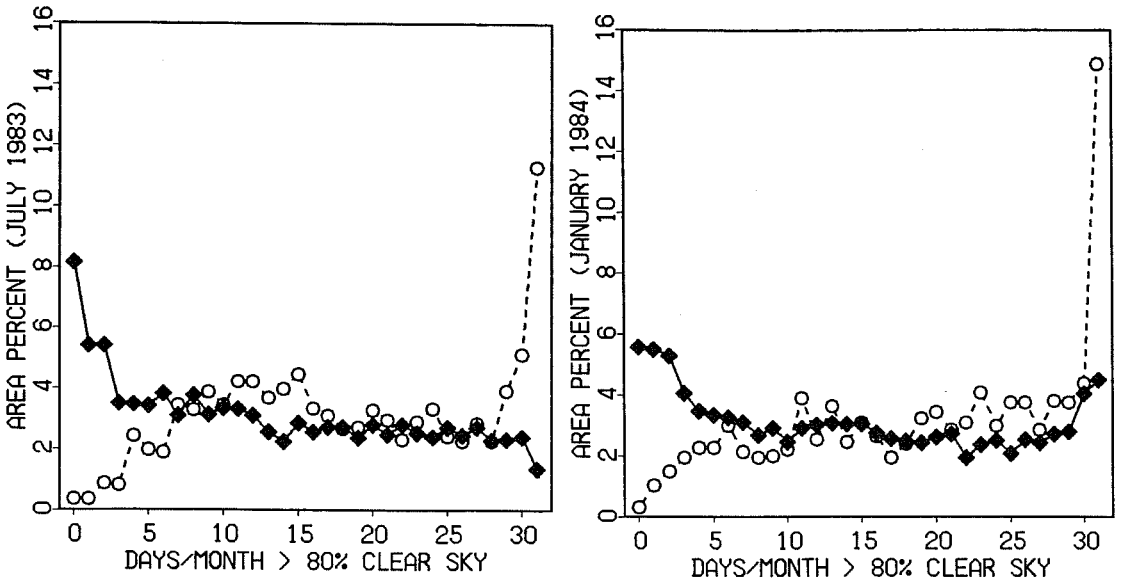

Fig. 9. (Left) Percent of land (open circles) and ocean (solid diamonds) surface as a function of the number of days per month (July 1983) when irradiance exceeded 80% of that under clear sky conditions. (Right) Similar data for January 1984. Results show that the oceans are consistently more cloud covered than land.

which meet the 80% criterion, but major differences are obvious (Figure 8). In July 1983, most of the subpolar North Pacific (north of the Kuroshio front at 40°N) was cloud covered 100% of the time. The transition between this perpetually cloudy region and the large area of almost perpetual sunny conditions centered on 20°N in the North Pacific is extremely well defined. The north Atlantic had more sunny days on average than the North Pacific at similar latitudes. In January 1984 the southern ocean between 50° and 65°S was also cloudy nearly 100% of the time. The warm ocean gyres were nearly always sunny. The perpetually sunny regions on land occur over the deserts, especially Africa and the Middle East. Fewer than five sunny days per month were found only in one or two isolated land spots (e.g., over the Amazon in January).

The frequency of cloudy days is very different over oceans and land (Figure 9). Combining data for July 1983 and January 1984, we found that approximately 11–14% of the ocean area had one or fewer sunny days. This contrasts with continents where less than 1.5% of the area had such conditions. At the opposite extreme, 30 or more days of sunshine occurred over 16–19% of the land surface but only over 4–9% of the ocean. Twenty-five percent of the ocean received 4 days or less of sunny weather, which contrasted with 10–11 days on land. Similarly, 50% of the ocean and land area received fewer than 11–13 and 17–20 sunny days, respectively. The fact that the temperate North Atlantic is sunnier on average than the North Pacific is most likely due to the effect of greater proximity of continental land masses on weather patterns.

Our second question regarding the persistence of solar irradiance over the ocean is partially answered by time series of Q_{TOT} computed from ISCCP data for July 1983 and July 1984 at ocean weather stations (OWS) B and I in the Atlantic and ocean station P and at 1°N, 140°W, in the Pacific (Figure 10). With the exception of OWS B, these areas are locations of recent, ongoing, or proposed investigations of ocean biogeochemical cycling processes. The reader is reminded that the data presented are representative of the 280 km x 280 km area containing the stations. Data from OWS I, located at 59°N just south of Iceland, suggest that surface solar irradiance is typically 50% of clear sky levels and is modulated on both short (2 day) and long (1–2 week) periods. The long-period fluctuation at this station appears seasonally coherent since the later parts of July 1983 and 1984 are very similar. Data from OWS B at nearly the same latitude (56°N) but in the western Atlantic show nearly twice the variability of light as at OWS I and a much less regular pattern. OWS P, in the eastern Pacific at 50°N, receives roughly the same light as at OWS I. The time series from 1°N, 140°W, in the Pacific shows almost totally clear conditions.

A population of phytoplankton at the equatorial Pacific location can expect nearly the same light field day after day. The light field at OWS P is next in order of consistency but this time is explained by perpetual cloudiness and is rarely interrupted by bright

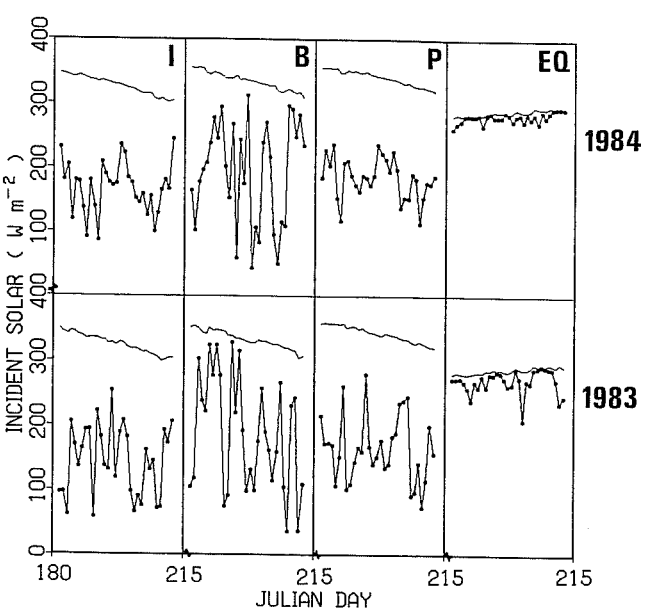

Fig. 10. Representative time series of solar irradiance for July 1983 and 1984 at ocean weather stations (OWS) I and B in the Atlantic and at OWS P and 1°N, 140°W, in the Pacific. These series illustrate the wide range in variability of surface solar irradiance over the ocean. Thin lines indicate estimated clear sky irradiances at these locations.

transients. OWS I is similar to OWS P in July. Contrasting with these stations, OWS B shows extremely high day-to-day variability. With ISCCP data it will be possible to address the question as to whether day-to-day variability of surface solar irradiance influences the geographic distribution of phytoplankton species. This is outside of the scope of the present paper.

4.2. Monthly and Interannual Statistics

Surface irradiance fields for the months of July 1983, January 1984, July 1984, and January 1985 (Figures 11–14) were derived to investigate differences in surface irradiance between oceans and land, differences between northern and southern hemisphere summers, and interannual differences. To aid this analysis, the world was categorized as "land," "coast," "seas, lakes and Arctic," "Atlantic," "Indian," and "Pacific," and zonal means were derived for the major land and ocean regions (Figure 15).

Interhemispheric differences. The comparison of July 1983 and January 1984 monthly mean maps reveals many of the same features already discussed in section 4.1. Differences among northern hemisphere land, Atlantic Ocean, and Pacific Ocean were found, with the Atlantic being more "continental" in nature than the Pacific. The Atlantic and Pacific oceans differ in zonal means from one another by as much as 80 W m^{-2} at 45°N during July 1983. Similarly, zonal ocean/continent differences may be up to 130 W m^{-2}. In contrast, in the southern summer (January 1984), little interocean difference is noted south of 15°S. The persistent band of circumpolar cloudiness centered at 60°S strongly attenuates incident solar irradiance by 50 to 60% compared with clear sky values. This factor of 2 irradiance decrease between 30°S and 60°S in all oceans is a consistent feature of the southern hemisphere.

The western South Atlantic is anomalous in several respects. In circumpolar waters, the Weddell Sea sector of the South Atlantic receives consistently greater irradiance (attenuated by only 30–40% from clear sky values) compared with the 50–60% reduction over other circumpolar current regions. The nutrient-rich subpolar waters of the Argentine basin also receive 20–30% greater irradiance than other ocean waters at the same latitude. These observations are consistent with the finding that both the Weddell Sea sector of the circumpolar current and the Argentine Basin are regions of relatively greater ocean primary productivity [*U.N. Food and Agriculture Organization (UN/FAO)*, 1972]. *Broecker and Takahashi* [1984] found that stronger than average deficits of surface pCO_2 relative to the atmosphere are found in the summertime in the same subpolar Argentine basin waters. These findings suggest that surface solar irradiance is a major determinant of the rate of carbon fixation by phytoplankton in nutrient-rich southern ocean waters.

Interannual differences. July 1983 was at the tail end of the 1982–1983 El Niño event (perhaps the strongest of the century). Was the interocean difference observed during July 1983 for the northern hemisphere a reflection of this fact? Zonally averaged data for July 1984 show that the basic interocean differences seen in July 1983 persist in the northern hemisphere but are somewhat reduced (Figure 15).

A map of the difference between July 1983 and July 1984 (Figure 16*a*) shows large scale patterns of interannual variability, especially over the Pacific Ocean. Consistent with the July 1983 El Niño pattern, the western tropical Pacific (centered on 8°N and 15°E) was much more cloud covered in 1983 than in 1984. This region (0–15°N and 110°E to 150°W) received between 25 and 75 W m^{-2} less during 1983. It is interesting that large scale differences of this magnitude were also found over large areas of the Pacific north of 25°N at 130°E on the west, and north of 30°N elsewhere. Differences of almost 100 W m^{-2} occurred over Japan coastal waters and over the northwest United States and western Canada. Equally important, there were positive differences (1983 higher) of 50 W m^{-2} over a broad region of the western Pacific centered at 20°N, 160°E. By comparison, little interannual difference was seen over the Atlantic, with the exception of a small area centered on 15°S, 0°W. The striking difference in interannual variability of the Atlantic and Pacific attests to the importance of the El Niño phenomenon in the Pacific. Over land, large positive differences (> 75 W m^{-2}) were found over northern Europe and eastern India.

The January 1984 minus January 1985 map shows a different pattern of interannual variability during the southern hemisphere summer (Figure 16*b*). Negative differences of up to 75 W m^{-2} were found in a large region of the tropical east Indian Ocean which extended across Australia into the western south Pacific. Smaller regions of 50 W m^{-2} differences were found in the circumpolar South Pacific region. A band of 50 W m^{-2} positive difference extends from the equator at 140°E to 10°S, 150°W. The strongest positive anomaly (> 75 W m^{-2}) is observed over southern Brazil and the southwest Atlantic in the region influenced by the South Atlantic Convergence Zone (SACZ). Although these differences over the ocean may seem small in terms of a percentage of clear sky irradiance (typically 350 W m^{-2}), they can be as high as 30–40% of irradiances typically received at the surface. The impact of such interannual variability of shortwave irradiance on the oceanic biosphere is as yet unquantified.

In summary, we have demonstrated that fundamentally different light regimes impact the ocean and land over time scales of days to years. We have also shown that the North Atlantic receives significantly greater irradiance than the Pacific. In the southern hemisphere, higher than average irradiance is found in the southwest Atlantic and the Weddell Sea sector of the southern ocean. In both these cases, proximity to land and its meteorological consequences seem to explain the differences observed. The role of such geographic differences in oceanic and terrestrial biospheric processes (in the present and in the past) is virtually unexplored owing to a data gap which ISCCP can now fill.

5. Conclusions

We have developed a computationally fast scheme for computing incident solar radiation at the surface using ISCCP data. The FAST scheme enables the production of a global data base which for the first time describes the daily variability of surface solar irradiance, the most important parameter forcing photosynthetic processes on land and in the ocean. The algorithm appears to be valid for all solar zenith angles and for both land and ocean surfaces. Tests against a full radiative transfer model showed a precision between 6 and 9 W m^{-2} for daily averages over a range of 0–400 W m^{-2} with best performance over the ocean. More tests are needed before the over all accuracy of the FAST method can be established. Towards this end, the FAST scheme will participate in the World Climate Research Program, Surface Radiation Budget April 1989 case study which includes a globally distributed set of some 20 stations where data comparable to the FIRE/SRB test (section 3.3) will be available. Further improvements in FAST now being implemented are the calculation of photosynthetically active irradiance (400–700 nm, typically 43–50% of solar irradiance) and the breakdown of irradiance into diffuse and direct components. These efforts will be reported separately.

The FAST algorithm using ISCCP data is much better than those depending on bulk formulae and cloud fraction alone [*Budyko*, 1963; *Reed*, 1977; *Dobson and Smith*, 1988] because it captures the extra variability, including with solar zenith angle, associated with

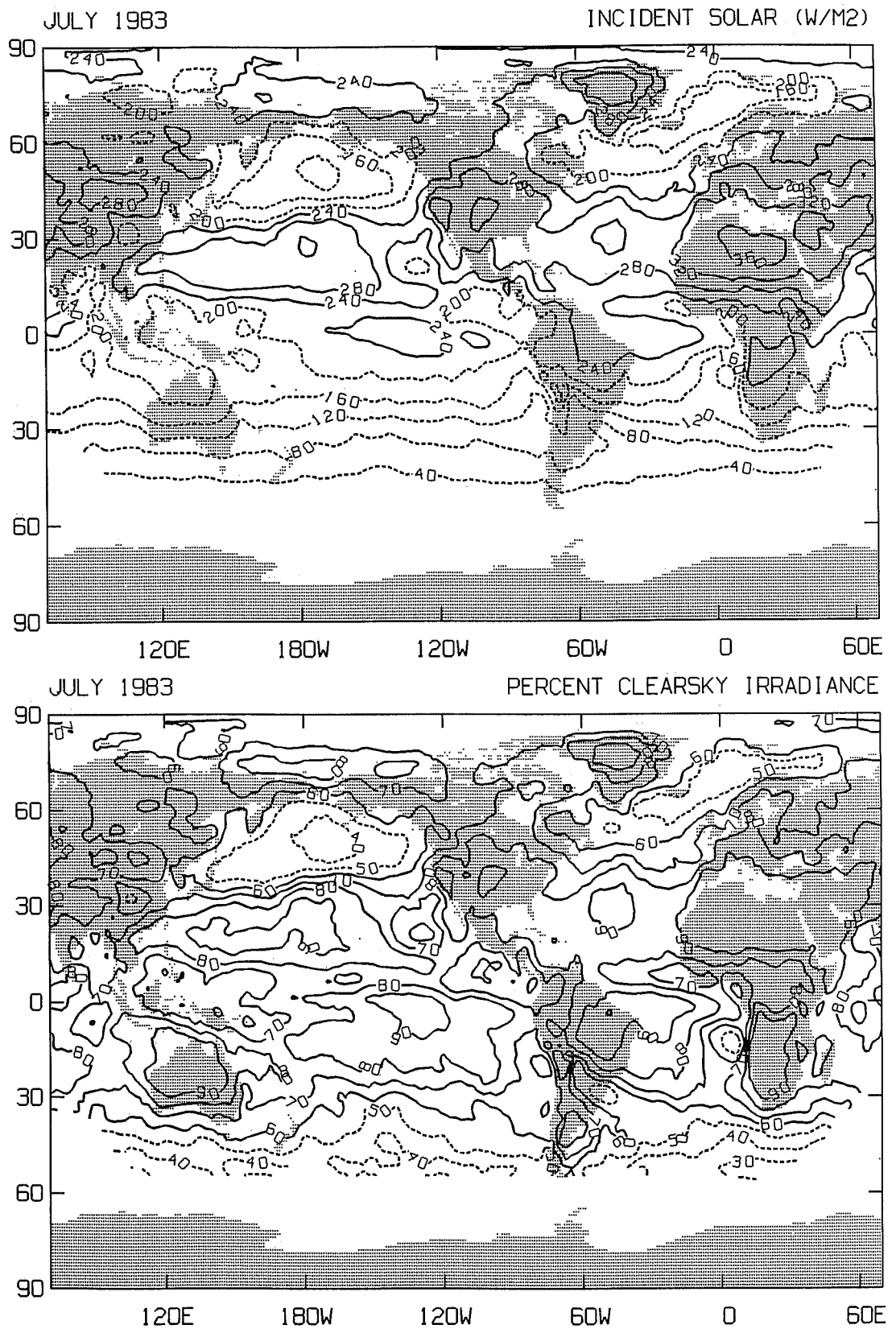

Fig. 11. Average monthly surface solar irradiance (in watts per square meter) and percentage of surface clear sky irradiance for July 1983 using the FAST scheme. Contours less than or equal to 200 W m^{-2} and 50% of clearsky irradiance are dashed.

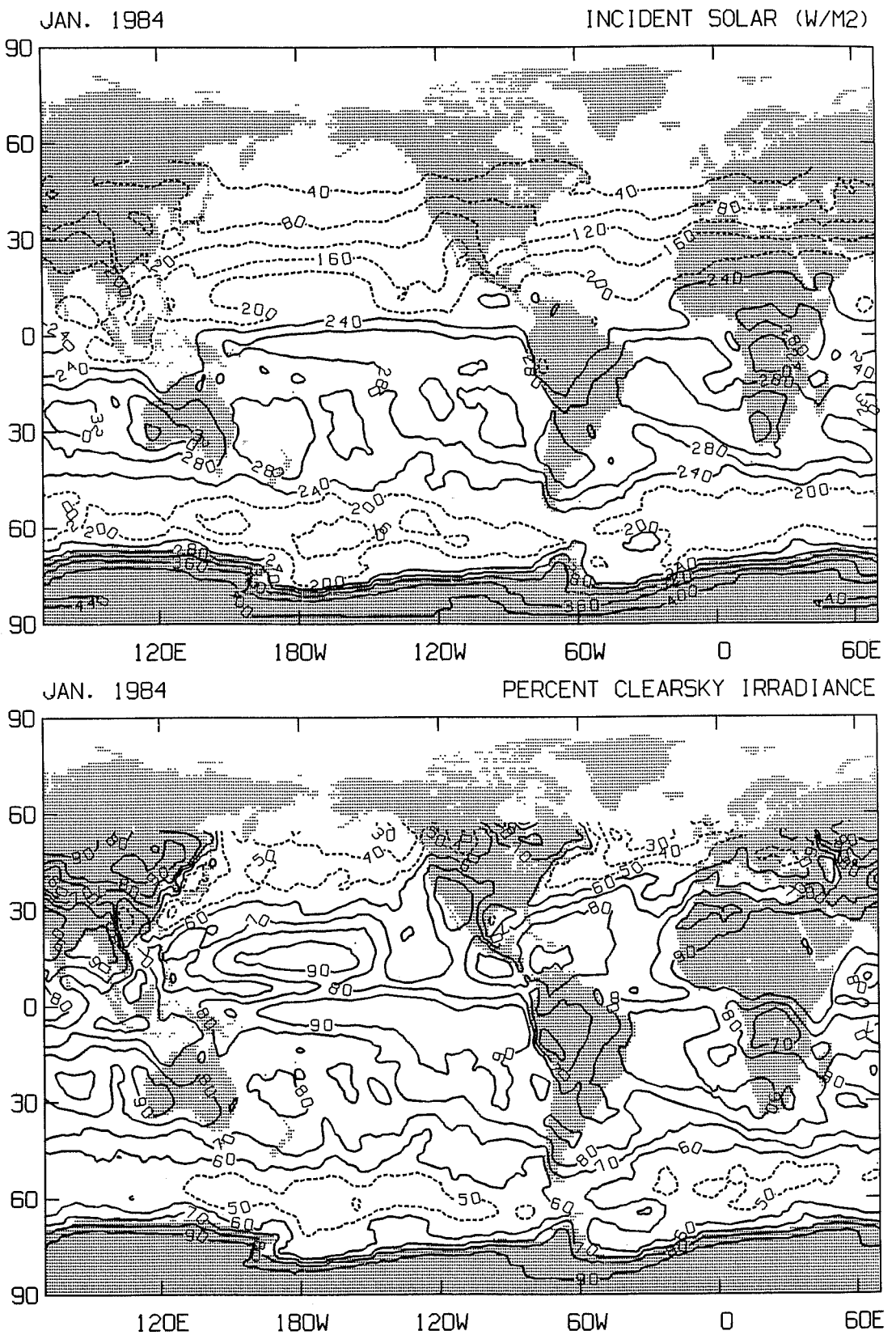

Fig. 12. Average monthly surface solar irradiance and percentage of surface clear sky irradiance for January 1984 using the FAST scheme.

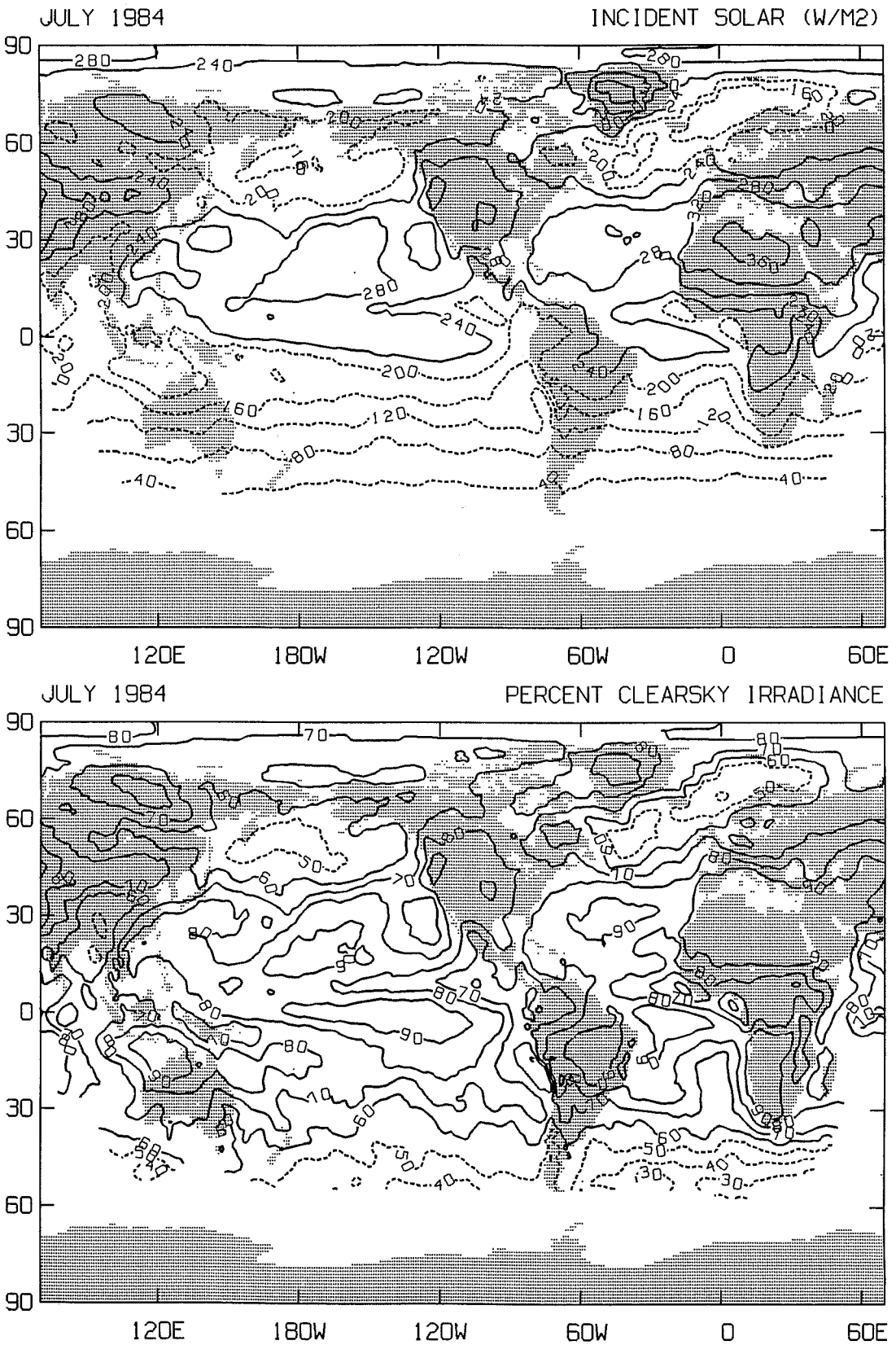

Fig. 13. Average monthly surface solar irradiance and percentage of surface clear sky irradiance for July 1984 using the FAST scheme.

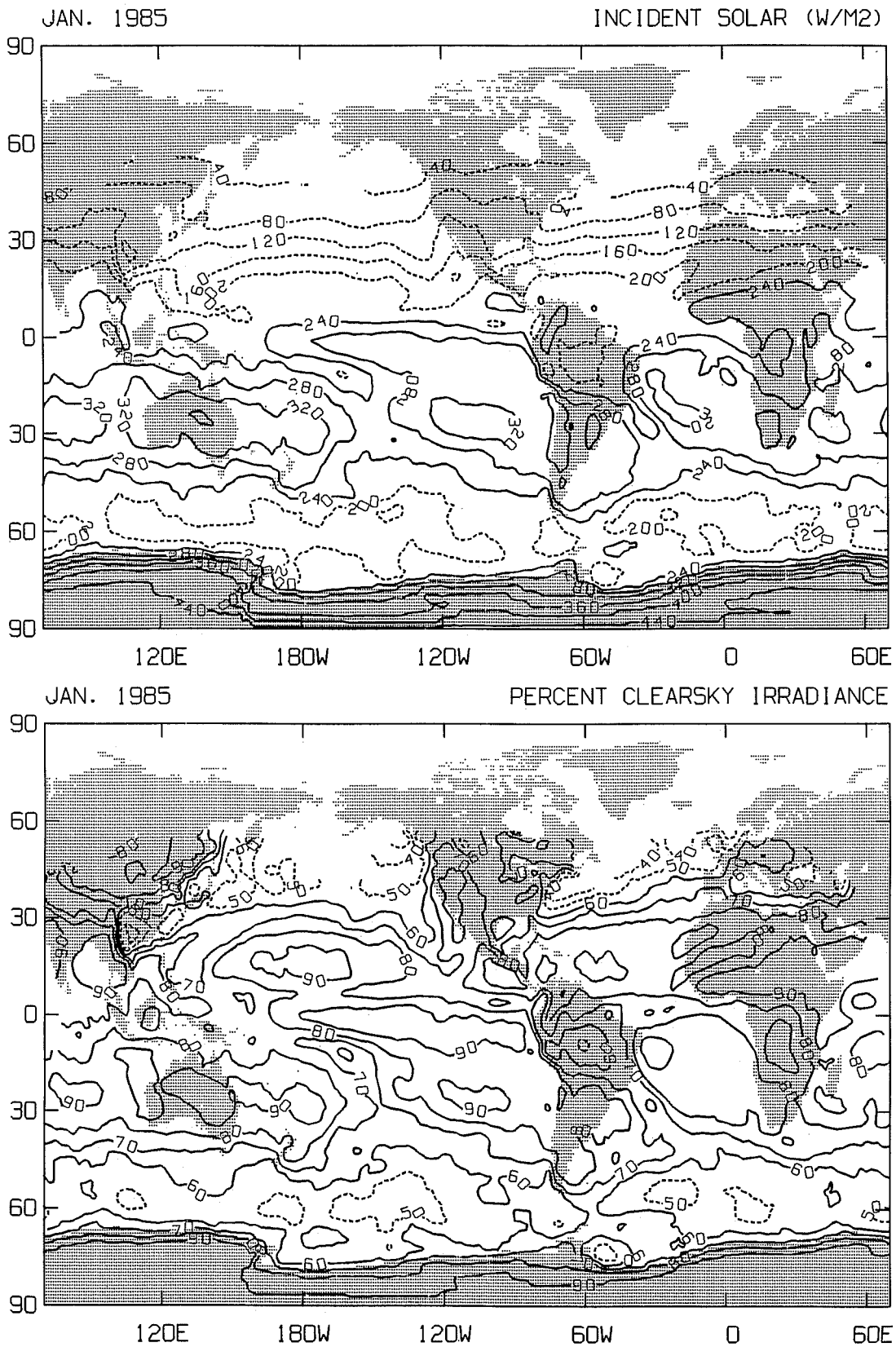

Fig. 14. Average monthly surface solar irradiance and percentage of surface clear sky irradiance for January 1985 using the FAST scheme.

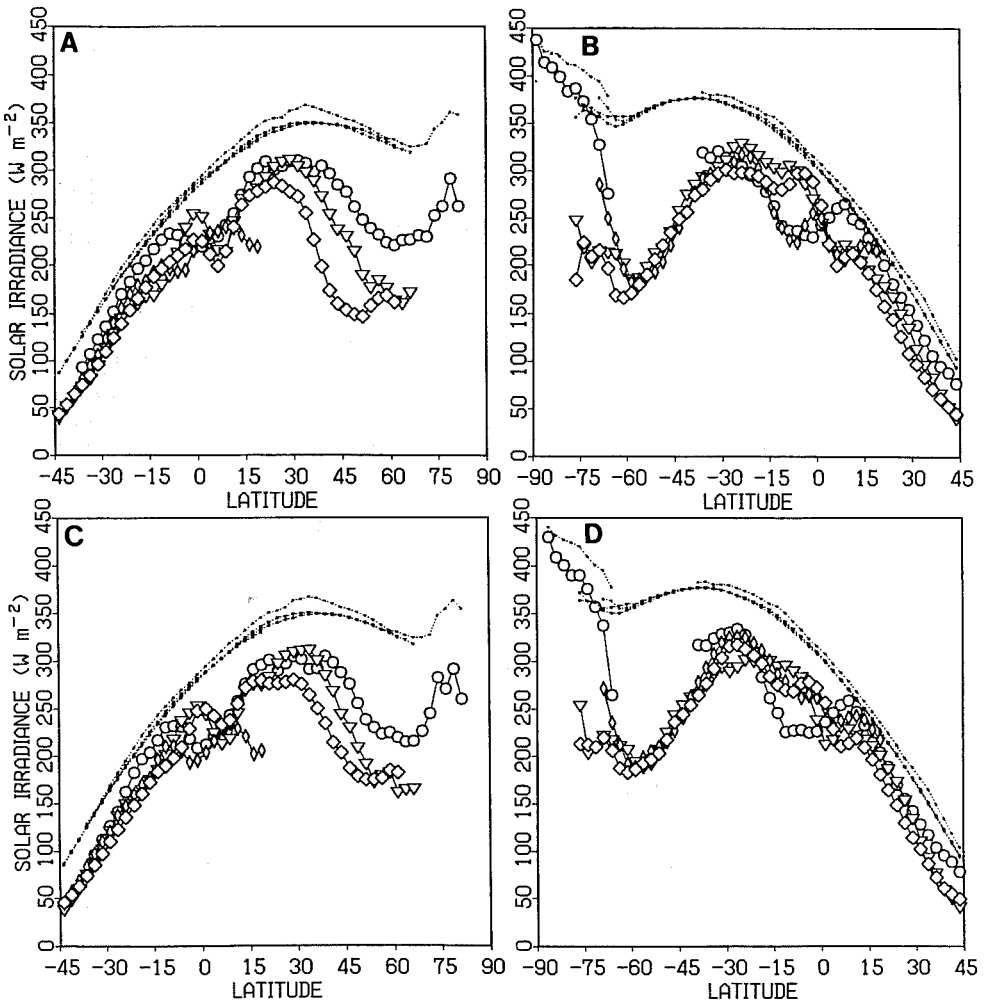

Fig. 15. Zonal average surface irradiance for land (open circles), Atlantic (open triangles), Indian (narrow diamonds), and Pacific (wide diamonds) oceans for (*a*) July 1983, (*b*) January 1984, (*c*) July 1984, and (*d*) January 1985 data. Clear sky values are denoted by dashed lines and are higher over land than over ocean. In summer, the northern oceans are significantly different from one another in terms of zonal irradiance, with the Atlantic being significantly brighter than the Pacific. Interocean differences are much smaller in the southern hemisphere.

varying cloud optical thickness. For application to data prior to ISCCP (July 1983), the bulk formula model of *Dobson and Smith* [1988] appears best for the ocean but can be improved in its representation of clear sky irradiance.

We have used the FAST algorithm with ISCCP data to illustrate temporal and spatial variability of surface solar irradiance over the globe. The light regimes experienced over the ocean are very different than over land. In July 1983, approximately 9% of the oceans surface was perpetually cloud covered, contrasting with only 0.3% over land. Certain oceanic regions (e.g., subpolar North Pacific) are perpetually cloudy. The basin-scale coastal zone color scanner images may be aliased on account of the inability of the satellite sensors to see the surface below such cloudy regions of the ocean [*McClain et al.*, 1990]. A continuous knowledge of the light field, coupled with a primary production model and the few CZCS surface pigment observations could significantly improve the estimation of oceanic productivity of such regions.

The Atlantic and Pacific oceans differ in zonal mean solar irradiance by as much as 80 W m^{-2} at 45°N during July 1983. This pattern of higher Atlantic irradiance is repeated in July 1984. Similarly, zonal irradiance at northern temperate latitudes may be up to 130 W m^{-2} higher over land than over the Pacific Ocean. The higher irradiance received by the Atlantic in the northern hemisphere during July appears to be due to greater continental influence. Regional interannual variability (July 1983 versus 1984) ranged between +100 and –100 W m^{-2}, especially in the Pacific Ocean. The variability, most likely related to the 1982–1983 El Niño event, was not only seen in the tropical Pacific ocean but on large scales over the entire North Pacific basin. These variations greatly exceed any errors found so far in FAST.

There is significant ongoing discussion about what controls the productivity of the nutrient-rich northern and southern ocean waters. One hypothesis receiving considerable attention is that iron availability limits the productivity [*Martin and Fritzwater*, 1988]. Another suggests that zooplankton grazing controls productivity [*Frost*, 1987]. The fact that these same regions are almost perpetually cloud covered and that there is a tantalizing correspondence between higher than average surface irradiance, productivity, and pCO_2 deficits in nutrient-rich areas of the south west Atlantic suggests that surface solar irradiance in its role both as a source of quanta for photosynthesis and as a part of the air-sea heat budget is a dominant player in the ocean biogeochemical cycle.

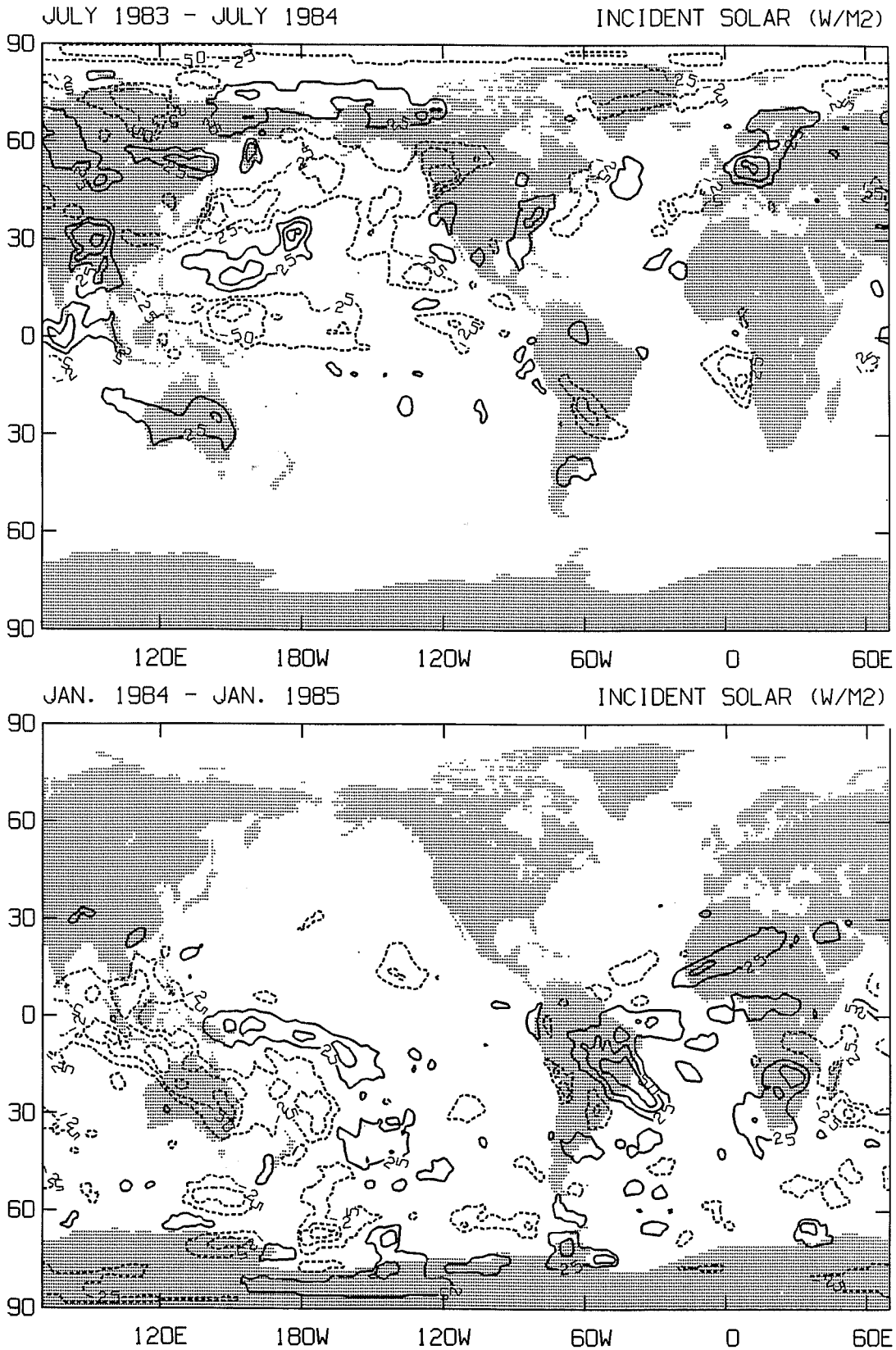

Fig. 16. (*a*) Map of irradiance differences (July 1983 minus July 1984). The fact that the majority of the differences over the ocean are found in the Pacific may be attributable to the fact that July 1983 was at the end of the 1982–1983 El Niño event. If true, El Niño effects extend significantly over the entire North Pacific. (*b*) Map of irradiance differences (January 1984 minus January 1985). As in Figure 16*a*, interannual differences ranged between + 100 and –100 W m^{-2}. Negative contours are dashed.

Acknowledgments. We acknowledge support through the NASA – Columbia University cooperative agreement NCC5-29A, NASA grant NAGW 2189, and the NASA Climate program. A. Lacis deserves special acknowledgment for the schemes for fast conversion between cloud optical thickness and solar zenith angle dependent and spherical albedos. Y. Zhang performed the FRT calculations and helped determine causes for differences. I. Fung and G. Russell contributed to our efforts. K.-R. Wang provided stimulation in the early stages of this work. Y. Kushnir, J. Marra, and R. Sambrotto are thanked for their comments on the manuscript. L-DGO contribution 4810.

REFERENCES

Balch, W.M., R.W. Eppley, and M.R. Abbott, Remote sensing of primary production II, A semi-analytical algorithm based on pigments, temperature and light, *Deep Sea Res.*, *36*, 1201–1217, 1989.

Berliand, T.C., Method of climatological estimation of global radiation (in Russian), *Meteorol. Gidrol.*, *6*, 9–12, 1960.

Bidigare, R.R., R.C. Smith, K.S. Baker, and J. Marra, Oceanic primary production estimates from measurements of spectral irradiance and pigment concentrations, *Global Biogeochem. Cycles*, *1*, 171–186, 1987.

Bishop, J.K.B., R.C. Smith, and K. Baker, Springtime distributions and variability of biogenic particulate matter in Gulf Stream warm-core ring 82B and surrounding N.W. Atlantic waters, *Deep Sea Res.*, in press, 1991.

Budyko, M.I., *Atlas of the Heat Balance of the World* (in Russian), 69 pp, Glavnaia Geofizicheskaia Observatoriia, Moscow, 1963. (English translation, I.M. Donehoo, Guide to the Atlas of the heat balance of the Earth, *WBT-106*, 22 pp., U.S. Weather Bur., Dep. of Commer., Washington, D.C., 1964.)

Bunker, A.F., Computations of the surface energy flux and annual air-sea interaction cycles of the north Atlantic ocean, *Mon. Weather Rev.*, *104*, 1122–1140, 1976.

Broecker, W.S., and T. Takahashi, Is there a tie between atmospheric CO_2 content and ocean circulation, in *Climate Processes and Climate Sensitivity, Geophys. Monogr. Ser.*, vol. 29, pp. 314–326, edited by J.E. Hansen and T. Takahashi, AGU, Washington D.C., 1984.

Chertok, B., Global monitoring of net solar irradiance at the ocean surface using Nimbus 7 satellite data, Ph.D. dissertation, 118 pp, Univ. of Calif., San Diego, 1989.

Darnell, W.L., W.F. Staylor, S.K. Gupta, and F.M. Dunn, Estimations of surface solar insolation using Sun-synchronous satellite data, *J. Clim.*, *1*, 820–835, 1988.

Dobson, F.W., and S.D. Smith, Bulk models of solar radiation at sea, *Q.J.R. Meteorol. Soc.*, *114*, 165–182, 1988.

Esaias, W.E., G.C. Feldman, C.R. McClain, and J.A. Elrod, Monthly satellite-derived phytoplankton pigment distribution for the North Atlantic Ocean Basin, *Eos Trans. AGU*, *67*, 835–837, 1986.

Esbensen S.K., and Y. Kushnir, The heat budget of the global ocean: An atlas based on estimates from surface marine observations, *Rep. 29*, 27 pp., 188 charts, Clim. Res. Inst., Oreg. State Univ., Corvallis, 1981.

Feldman, G.C., et al., Ocean color: Availability of the global data set, *Eos Trans. AGU*, *70*, 634–641, 1989.

Frost, B.W., Grazing control of phytoplankton stock in the open subarctic Pacific Ocean: A model assessing the role of mesozooplankton, particularly the large calanoid copepods *Neocalanus* spp. *Mar. Ecol. Prog. Ser.*, *39*, 49–68, 1987.

Frouin, R., D.W. Lingner, C. Gautier, K.S. Baker, and R.C. Smith, A simple analytical formula to compute clear sky total and photosynthetically available solar irradiance at the ocean surface, *J. Geophys. Res.*, *94*, 9731–9742, 1989.

Gautier, C., G.R. Diak, and S. Masse, A simple physical model to estimate incident solar radiation at the sea surface from GOES satellite data, *J. Appl. Meteorol.*, *19*, 1005–1012, 1980.

Goldman, J.C., and J.J McCarthy, Steady state growth and ammonium uptake by a fast growing marine diatom, *Limnol. Oceanogr.*, *22*, 932–936, 1978.

Hansen, J.E., and L. Travis, Light scattering in planetary atmospheres, *Space Sci. Rev.*, *16*, 527–610, 1974.

Hansen, J.E., G. Russell, D. Rind, P. Stone, A. Lacis, S. Lebedeff, R. Reudy, and L. Travis, Efficient three-dimensional global models for climate studies: Models I and II, *Mon. Weather Rev.*, *111*, 609–662, 1983.

Isemer, H.-J., and L. Hasse, *The Bunker Climate Atlas of the North Atlantic Ocean*, vol. 2,: *Air-Sea Interactions*, 252 pp., Springer-Verlag, New York, 1987.

Lacis, A.A., and J.E. Hansen, A parameterization for the absorption of solar radiation in the Earth's atmosphere, *J. Atmos. Sci.*, *31*, 118–133, 1974.

Lacis, A.A., and V. Oinas, A description of the correlated *k* distribution method for modeling non-gray gaseous absorption, thermal emission, and multiple scattering in vertically inhomogeneous atmospheres., *J. Geophys. Res.*, *96*, 9027–9063, 1991.

Langdon, C., On the causes of interspecific differences in the growth-irradiance relationship for phytoplankton, II, A general review, *J. Plankton. Res.*, *10*, 1291–1312, 1988.

Marra, J., R.R. Bidigare, and T.D. Dickey, Nutrients and mixing, chlorophyll and phytoplankton growth, *Deep Sea Res.*, *37*, 127–143, 1990.

Martin, J.H., and S.E. Fritzwater, Iron deficiency limits phytoplankton growth in the north-east Pacific subarctic, *Nature*, *331*, 341–343, 1988.

McClain, C.R., G.C. Feldman, W.E. Esaias, J.K. Firestone, and M. Darzi, Meteorological forcing of biological processes in the North Atlantic ocean, paper presented at 2nd International Conference on Oceans From Space, Int. Assoc. for the Phys. Sci. of the Oceans, Venice, Italy, 1990.

McClatchey, R.A., W.S. Benedict, S.A. Clough, D.E. Burch, R.F. Calfee, K. Fox, L.S. Rothman and J.S. Garing, AFCRL atmospheric absorption line parameters compilation, *Environ. Res. Pap. 434*, 78 pp, Hanscom Air Force Base, Bedford, Mass., 1973.

Minnis, P., and E.F. Harrison, Diurnal variability of regional cloud and clear sky radiative parameters derived from GOES data, I, Analysis method, *J. Clim. Appl. Meteorol.*, *23*, 993–1011, 1984.

Platt, T., Primary production of the ocean water column as a function of surface light intensity: Algorithms for remote sensing, *Deep Sea Res.*, *33*, 149–164. 1986.

Raschke, E., A. Gratzki, and M. Rieland, Estimates of global radiation at the ground from the reduced data sets of the international satellite cloud climatology project, *J. Climatol.*, *7*, 205–213, 1987.

Reed, R.K., On estimating insolation over the ocean, *J. Phys. Oceanogr.*, *7*, 482–485, 1977.

Reed, R.K. An estimate of the climatological heat fluxes over the tropical Pacific ocean, *J. Clim. Appl. Meteorol.*, *24*, 833–840, 1985.

Rossow, W.B., and A.A. Lacis, Global, seasonal cloud variations from satellite radiance measurements, II, Cloud properties and radiative effects, *J. Clim.*, *3*, 1204-1253, 1991.

Rossow, W.B., and R.A. Schiffer, ISCCP cloud data products, *Bull. Am. Meteorol. Soc.*, *72*, 2–20, 1991.

Rossow, W.B., et al., ISCCP cloud algorithm intercomparison, *J. Clim. Appl. Meteorol.*, *24*, 877–903, 1985.

Rossow, W.B., L.C. Garder, P-J. Lu, and A.W. Walker, International Satellite Cloud Climatology Project (ISCCP) documentation of cloud data. *WMO/TD-No. 266*, 78 pp. + 2 appendices, World Meteorol. Organ., Geneva, 1988.

Rossow, W.B., Y. Zhang, and A.A. Lacis, Calculations of atmospheric radiative flux profiles, paper presented at the Seventh Conference on Atmospheric Radiation, Am. Meteorol. Soc., San Francisco, Calif., July 23–27, 1990.

Rothman, L.S., AFGL atmospheric absorption line parameters compilation: 1980 version, *Appl. Opt.*, *20*, 791–794. 1981.

Sathyendranath, S., and T. Platt, The spectral irradiance field at the surface and in the interior of the ocean: A model for applications in oceanography and remote sensing, *J. Geophys. Res.*, *93*, 9270–9280, 1988.

Sathyendranath, S., T. Platt, C.M. Caverhill, R.E. Warnock, and M.R. Lewis, Remote sensing of oceanic primary production: Computations using a spectral model, *Deep Sea Res.*, *36*, 431–453, 1989.

Schiffer, R.A., and W.B. Rossow, The international satellite cloud climatology project (ISCCP): The first project of the World Climate Research Programme, *Bull. Am. Meteorol. Soc.*, *64*, 779–784, 1983.

Schiffer, R.A., and W.B. Rossow, ISCCP global radiance data set: A new resource for climate research, *Bull. Am. Meteorol. Soc.*, *66*, 1498–1505, 1985.

Sheldon, R.W., A. Prakash, and W.H. Sutcliffe, Jr., The size distribution of particles in the ocean, *Limnol. Oceanogr.*, *17*, 327–340, 1972.

Smith, S.D., and F.W. Dobson, The heat budget at ocean weather station Bravo, *Atmos. Ocean*, *22*, 1–22, 1984.

Stuhlmann, R., M. Rieland, and E. Raschke,. An improvement of the IGMK model to derive total and diffuse solar radiation at the surface from satellite data, *J. Appl. Meteorol.*, *29*, 586-603, 1990.

Sverdrup, H.U., On conditions for vernal blooming of phytoplankton, *J. Cons., Cons. Int. Explor. Mer.*, *18*, 287–295, 1953.

Tarpley, J.D., Estimating incident solar radiation at the surface from geostationary satellite data, *J. Appl. Meteorol.*, *18*, 1172–1181, 1979.

Tucker, C.J., and P.J. Sellers., Satellite remote sensing of primary production. *Int. J. Remote Sens.*, *7*, 1395–1416, 1986.

Toon, O.B., and J.B. Pollack, A global average model of atmospheric aerosols for radiative transfer calculations, *J. Appl. Meteorol.*, *15*, 225–246, 1976.

U.N. Food and Agriculture Organization (UN-FAO), Atlas of the Living Resources of the Seas. Department of Fisheries, Rome, 1972.

Whitlock, C.H., et al., Comparison of surface radiation budget satellite algorithms for downwelled shortwave irradiance with Wisconsin FIRE/SRB surface-truth data, papers presented at the Seventh Conference on Atmospheric Radiation, Am. Meteorol. Soc., San Francisco, July 23–27, 1990.

Willson, R.C., Accurate solar "constant" determination by cavity pyrheliometers, *J. Geophys. Res.*, *83*, 4003–4007, 1978.

Wroblewski, J.S., J.L. Sarmiento, and G.R. Flierl, An ocean basin scale model of plankton dynamics in the North Atlantic, 1, Solutions for the climatological oceanographic conditions in May. *Global Biogeochem. Cycles*, *2*, 199–218,. 1988.

J. K. B. Bishop, Lamont–Doherty Geological Observatory, Columbia University, Palisades, NY 10964.

W. B. Rossow, NASA Goddard Institute for Space Studies, New York, NY 10025.

(Received April 3, 1991;
revised July 1, 1991;
accepted July 1, 1991.)